Universidade do Minho
Escola de Ciências

Cristiana Filipa Barreiro da Cunha

Polymeric micelles for delivery of antimicrobial peptides

November 2020

Cristiana Cunha **Polymeric micelles for delivery of antimicrobial peptides**

UMinho | 2020

UNIVERSITY OF COPENHAGEN

Erasmus+

Universidade do Minho
Escola de Ciências

Cristiana Filipa Barreiro da Cunha

Polymeric micelles for delivery of antimicrobial peptides

Master's Dissertation
Master in Biophysics and Bionanosystems

Work developed under supervision of
André Costa, PhD
Hanne Mørck Nielsen,
Professor, PhD

November 2020

Direitos De Autor E Condições De Utilização Do Trabalho Por Terceiros

Este é um trabalho académico que pode ser utilizado por terceiros desde que respeitadas as regras e boas práticas internacionalmente aceites, no que concerne aos direitos de autor e direitos conexos.

Assim, o presente trabalho pode ser utilizado nos termos previstos na licença abaixo indicada.

Caso o utilizador necessite de permissão para poder fazer um uso do trabalho em condições não previstas no licenciamento indicado, deverá contactar o autor, através do RepositóriUM da Universidade do Minho.

Licença concedida aos utilizadores deste trabalho

Atribuição-NãoComercial-SemDerivações

CC BY-NC-ND

https://creativecommons.org/licenses/by-nc-nd/4.0/

Acknowledgments

The experimental part of this project was carried out at the University of Copenhagen, Denmark, Faculty of Health and Medical Sciences in the Drug Delivery and Biophysics of Biopharmaceuticals group within an *Erasmus Placement* programme, from September 2019 to July 2020.

I would like to give a sincere thanks to my supervisor Professor Hanne Mørck Nielsen (Department of Pharmacy, University of Copenhagen) for all scientific discussions, valuable feedback, motivation and kind support. Also, I would like to acknowledge Junior Researcher André Costa (Centre of Molecular and Environmental Biology, Department of Biology, University of Minho) for his valuable contribution as my co-supervisor, scientific input, his patience and availability to help.

I also want to express my gratitude to Postdoctoral Researcher Sylvia Kłodzińska for all scientific discussions, valuable feedback and guidance in the laboratory. For that and also for the enthusiastic involvement in my project, for the encouragement and great support, but especially for believing in my capabilities sometimes even more than myself. Furthermore, I wish to thank Danai-Anastasia Panou for allowing me to work with her, outside of the scope of this project, performing transport studies and extending my scientific knowledge.

A special thanks to all people that I had the pleasure to work with during my time working in Nielsen group, for the pleasant and a fun working atmosphere. I also would like to extend my gratitude to all my Professors during my Master of Biophysics and Bionanosytems, in special Professor Andreia Gomes for all the patience and help during these last years.

Furthermore, I would like to thank my family and friends, for the support, motivation and for always being there for me.

Final, I would like to thank the University of Copenhagen and the University of Minho.

STATEMENT OF INTEGRITY

I hereby declare having conducted this academic work with integrity. I confirm that I have not used plagiarism or any form of undue use of information or falsification of results along the process leading to its elaboration.

I further declare that I have fully acknowledged the Code of Ethical Conduct of the University of Minho.

Polymeric micelles for delivery of antimicrobial peptides

Abstract

Antimicrobial resistance is one of the most serious threats to human health in this century, causing significant economic burden and high mortality. Without effective antimicrobial therapies, the number of deaths associated with infections will continue to rise inexorably. This prospect has prompted the search for therapeutic alternatives, such as antimicrobial peptides (AMPs). However, non-specific toxicity, low stability and short half-life hinder the development of AMPs into stand-alone medicines, limiting their potential as powerful antimicrobial agents. These challenges can be overcome by utilizing novel formulation strategies, such as nanogels or polymeric micelles for the delivery of such peptides.

In this project, oleic-grafted hyaluronan (OL-HA) polymeric micelles for the encapsulation of the antimicrobial cell penetration peptides L- and D-PenetraMax and its lipidated version Syn-2 were developed and characterized. With the optimized method, it was possible to prepare small anionic micelles, with a hydrodynamic diameter range of 100 – 300 nm, capable of efficiently loading all three peptides. High values of encapsulation efficiency were found but at the expense of a slower release profile. L-PenetraMax showed to be very prone to degradation and its encapsulation did not improve this behaviour. The polymeric micelles, despite the very slow release, effectively reduced the peptide cytotoxicity towards hepatic, endothelial, intestinal and red blood cells (RBCs), while maintaining their antimicrobial activity against *Escherichia coli*, *Pseudomonas aeruginosa* and *Staphylococcus aureus*. Additionally, the polymeric micelles prepared also seemed capable of prevent biofilm growth at concentrations higher than the minimal inhibitory concentration (MIC) values. These findings support the use of OL-HA polymeric micelles to increase the safety of peptides with antimicrobial properties to intravenous administration.

Keywords: Oleic-grafted hyaluronan; Polymeric micelles; Cell-penetrating peptides; Antimicrobial peptides

Micelas poliméricas para entrega de péptidos antimicrobianos

Resumo

A resistência antimicrobiana é uma das ameaças mais sérias à saúde humana deste século, causando uma carga económica significativa e alta mortalidade. Sem terapias eficazes, o número de mortes associadas a infeções por espécies resistentes a antibióticos continuará a aumentar inexoravelmente. Esta perspetiva tem motivado a busca por terapias alternativas, como por exemplo o uso de péptidos antimicrobianos. No entanto, a toxicidade não específica, a baixa estabilidade e curto tempo de vida dos péptidos dificultam o seu desenvolvimento em medicamentos por si só, limitando o seu potencial como poderosos agentes antimicrobianos. Esses desafios podem ser superados utilizando novas estratégias de formulação, tais como nanogéis ou micelas poliméricas para a entrega de péptidos antimicrobianos.

Neste projeto, foram desenvolvidas e caracterizadas micelas poliméricas à base de hialuronato oleico para a encapsulação de péptidos antimicrobianos capazes de penetrar membranas celulares, L- e D-PenetraMax e a sua versão lipidada Syn 2. Com o método otimizado, foi possível preparar pequenas micelas aniónicas, com diâmetro hidrodinâmico entre 100 e 300 nm, capazes de encapsular eficientemente os três péptidos referidos. Apesar dos elevados valores de eficiência de encapsulamento, as micelas apresentaram um perfil de libertação mais lento. O péptido L-PenetraMax mostrou ser bastante suscetível à degradação e o seu encapsulamento nas micelas não melhorou esse comportamento. As micelas poliméricas reduziram eficazmente a citotoxicidade dos péptidos em células hepáticas, endoteliais, intestinais e em eritrócitos, mantendo a sua atividade antimicrobiana contra *Escherichia coli*, *Pseudomonas aeruginosa* e *Staphylococcus aureus*. Adicionalmente, estas micelas poliméricas também mostraram ser capazes de prevenir o crescimento de biofilme bacteriano a concentrações superiores aos valores de concentração mínima inibitória (MIC). Estes resultados apoiam o uso destas micelas poliméricas à base de hialuronato para melhorar o uso seguro dos péptidos mantendo as propriedades antimicrobianas para administração intravenosa.

Palavras-chave: Hialuronato oleico; Nanopartículas poliméricas; Péptidos de penetração celular; Péptidos antimicrobiais

Contents

List of Abbreviations

2-ProH – 2-Propanol

AA – Amino acid

AgNPs – Silver nanoparticles

AMPs – Antimicrobial peptides

AMR – Antimicrobial resistance

API-PUL – Amaranth protein isolate-pullulan

AuNPs – Gold nanoparticles

CNTs – Carbon nanotubes

CPPs – Cell-penetrating peptides

DLS – Dynamic light scattering

EE – Encapsulation efficiency

EPR – Enhanced permeation and retention

GAG – Glycosaminoglycan

HA – Hyaluronic acid

IFN-β– Interferon-β

MAP – Membrane active peptide

MIC – Minimal inhibitory concentration

OL-HA – Oleic-grafted hyaluronan

PDI – Polydispersity Index

PEG – Polyethylene glycol

Pen – Penetratin

PLGA – Polylactic-co-glycolic acid

Pmax - PenetraMax

RBC - Red blood cells

SD – Standard deviation

SiNPs – Silica nanoparticles

TEM – Transmission electron microscopy

ZP – Zeta potential

Bacteria

E. coli – Escherichia coli

P. aeruginosa – Pseudomonas aeruginosa

S. aureus – Staphylococcus aureus

For amino acids standard IUPAC single letter nomenclature is applied.

List of Figures

List of Tables

1. Introduction

1.1. Antimicrobial Resistance

Antimicrobial resistance (AMR), which is the ability of microorganisms to withstand antimicrobial treatments, is one of most serious health threats of the 21st century, becoming a global public health problem that requires action across all government sectors and society (1). Among all microorganisms, bacteria are the most concerning group, as recent estimates based on data from EARS-Net (European Antimicrobial Resistance Surveillance Network) show that each year, more than 670 000 infections occur in the European Region due to an infection with a resistant bacterial strain (2). These numbers are continuously increasing as bacteria continue to develop resistance to available antibiotics, and the amount of deaths associated with such infections is expected to reach 10 million deaths worldwide by 2050 (2,3).

AMR is a natural microbiological phenomenon. Over the course of billions of years, bacteria have developed mechanisms to fight for their survival. Misuse of antibiotics, non-prescription use of antibiotics, skipping doses, saving and sharing antibiotics, could contribute to the development to resistant bacteria by exposing the pathogens to sub-inhibitory antibiotic concentrations (4,5). When exposed to such low antibiotic concentrations, bacterial resistance can occur through a decrease in the drug permeability, biofilm formation, active efflux pumps, and even immune-evasive tactics, among other mechanisms (5,6).

The Infectious Diseases Society of America has highlighted a faction of antibiotic resistant bacteria (*Enterococcus faecium*, *Staphylococcus aureus*, *Klebsiella pneumoniae*, *Acinetobacter baumannii*, *Pseudomonas aeruginosa* and *Enterobacter* spp.), pathogens also known by the acronym ESKAPE (7,8). These pathogens are a particular threat, as they quickly develop resistance to effectively "escaping" a large number of antibacterial drugs, including carbapenems and third generation cephalosporins, which are currently the best available antibiotics for treating multidrug resistant bacteria (9,10). Since 2017, only eight new antibiotics have been approved (11). However, these mostly belong to known antibiotic classes and thus are not entirely new entities. There were, in 2019, 50 antibiotics and combinations, as well as 10 biological drugs in clinical trials (11). Despite public investment in the development of antibacterial agents has increased in recent years, the current pipeline remains insufficient (11). In fact, the average progression rates, the clinical development duration and the high cost of clinical trials has led several pharmaceutical companies to ditch R&D in new antimicrobials (12). Without effective antibiotics, the success of surgical procedures such as organ transplants and caesarean sections or even chemotherapy will be compromised, resulting in

prolonged hospital stays and increased mortality (5,13). Over the past decades, the World Health Organization has been leading multiple initiatives to address antimicrobial resistance, giving technical assistance to help countries develop their national action plans, and reinforce their health and surveillance systems.

1.2. Novel therapies against antimicrobial resistance

With the scarce development of new antibiotics (11), researchers around the world also focus on addressing the issue of antimicrobial resistance with different approaches. Application of novel therapies, such as combination therapy using different antibiotics and/or antimicrobial adjuvants, bacteriophages and photodynamic therapy, antimicrobial peptides (AMPs), antibacterial antibodies, phytochemicals and nanoparticles as antibacterial agents are being studied and applied in clinical environments (14–16).

The combination therapy helps in overcoming the vulnerabilities of the existing antimicrobials by supplementing them, either with other antibiotic or with adjuvants targeting important metabolic pathways (permeabilizers, lactamase inhibitors, efflux pump inhibitors, quorum sensing inhibitors, toxin inhibitors etc.) (14). Other kinds of entities that could also be used in combination therapies are the non-antibiotic agents that exhibit antimicrobial activity via multiple and different mechanisms of action, such as non-steroidal anti-inflammatory drugs, local anaesthetics or phenothiazines (17). Bacteriophages, viruses that specifically infect bacteria through recognition of a cell surface receptor, present one of the most attractive alternatives to combating antimicrobial resistance with already some preparations commercially available (4,14). Stafal (Bohemia Pharmaceuticals, Slovakia), Sextaphage (Microgen, ImBio Nizhny Novgorod, Russia) and Pyophage (Georgian Eliava Institute of Bacteriophage, Microbiology, and Virology) are formulations against multi-drug resistance pathogens (14). The major problem with this therapy is that is confined only to certain parts of the globe (16). Additionally, reports have shown that bacteriophages may induce biofilm formation in some bacteria (18).

In addition to the growing concern in searching and evaluating the clinical potential of the alternative therapies mentioned above, research on combinatorial approach is also becoming more attractive. Nanotechnology has already shown great potential in the antimicrobial field, with more than 10 nanoparticle-based products marketed for the bacterial diagnosis, antibiotic delivery and medical devices (19–21). With unique but diverse physicochemical characteristics, nanomaterials can also be used in combination with different antimicrobial strategies for more specific targeting approaches. Nanomaterials can work as delivery systems for existing antimicrobial agents, or by taking advantage of their possible antimicrobial properties

(22–24). The present work aims to evaluate whether a synergetic effect, higher bioavailability and enhanced antimicrobial properties can be obtained using hyaluronic acid-based (HA-based) nanoparticles to delivery cell penetrating peptides (CPPs) with antimicrobial properties.

1.2.1. Membrane active peptides

Membrane active peptides (MAPs) are a highly diverse group of natural or synthetic peptides, with the ability to interact with biological membranes due to their physicochemical properties (25,26). AMPs and CPPs, both usually short and positively charged, belong to the MAP family but differ in their biological functions (27). CPPs have the ability to cross cell membranes and deliver macromolecular cargo, while AMPs are able to kill or inhibit the growth of bacteria (28). Their function depends on the lipid composition of the target membrane (29), on their secondary structure, amino acid sequence and even concentration (25,27,28). Because of their different functions, CPPs and AMPs have been separated for a long period, but recent investigations have shown that there are many MAPs with dual functionality, specifically antimicrobial and cell-penetrating properties (25,30–33). This brings to attention the exciting possibility of using CPPs, a group of peptides previously explored only for their permeation enhancement properties, as antimicrobial agents, effectively broadening the amount of potential new antibiotics.

1.2.1.1. Antimicrobial Peptides

AMPs are a diverse class of naturally occurring antibiotics that have been studied over the past decades and that are associated with a reduced risk of resistance development (34). AMPs are part of the innate immune system of all living organisms, representing an ancient host defence mechanism against a wide range of pathogens, including bacteria, viruses, fungi yeast and protozoa (34,35). These peptides are usually short, typically < 50 amino acids (AAs), (36–39) cationic and amphipathic, with hydrophobic percentages between 31 – 70% (35,40–42). AMPs have a beneficial range of functions: from killing bacteria to immune modulation (43–45), prevention of biofilm formation (24), as well as anticancer (39) or antiviral properties (47). These activities are dependent on the AMPs structural characteristics and amino acid sequence, for example, the initial interaction with the negatively charged membrane surface of the bacteria is mainly attributed to the positive charge of the AMP (40,42,48). Although many different modes of action have been described for AMPs, all rely on electrostatic interactions between the peptide and the bacterial cell membrane

and subsequent destabilization and permeabilization of the cells. This mode of action is very efficient, reducing the bacterial ability to develop resistance, as the metabolism of the peptides is not required for antimicrobial action since most of them act by disrupting the cell membrane without needing a receptor (14,42,49). Another key characteristic of AMPs that influences activity is the peptide hydrophobicity, which is capable of modulating the antimicrobial efficiency and influencing toxicity towards mammalian cells (42). Despite the multiple beneficial characteristics of AMPs as antimicrobial therapeutics, there are some disadvantages associated with these peptides that need to be addressed. These include low stability due to chemical and biological degradation, unfavourable pharmacokinetics, rapid clearance, as well as hemolytic toxicity due to higher cationic charges and cytotoxicity when very hydrophobic peptides are used (40,42,50–52).

1.2.1.2. Cell penetrating peptides

Initially, this group of peptides were known as protein transduction domains, a specific amino acid sequence present in some proteins and necessary for the internalization into the cells to occur (26,33). The first identified sequences were tat (GRKKRRQRRRPPQ) from the HIV-1 transactivator of transcription protein (53) and penetratin (RQIKIWFQNRRMKWKK) from the Antennapedia homeotic transcription protein (54). Since then, almost 2000 CPPs were identified and intensively studied and compiled in the online database CPPsite 2.0[1] (55). CPPs are defined as predominantly cationic and with short sequences of up to 40 AAs, capable of internalizing cargos into living cells in a non-destructive manner by various passive and active mechanisms (31,56). Because of this ability, CPPs can facilitate the delivery of diverse therapeutic biomolecules and enable access to intracellular targets with low cytotoxicity (31,55–58). It was demonstrated *in vitro* and *in vivo* that CPPs are capable of efficient cellular import of peptides (59), proteins (60), nucleic acid (61–63) (pDNA, siRNA, miRNA), small molecule drugs (64), fluorophores (65), hard nanoparticles (66,67) as well as soft nanoparticles, such as liposomes (68) or micelles (69). CPPs show a great variety in terms of amino acid composition and 3D structure, resulting in different modes and levels of uptake. Endocytosis and direct translocation through the cellular membrane are the major uptake mechanisms, that depend on the cell line, the cargo type, CPP concentration and even the way the cargo is attached to the CPP, covalently or non-covalently (70).

[1] http://crdd.osdd.net/raghava/cppsite/

Although several different criteria have been proposed for the classification of CPPs, these peptides can be simply categorized into 3 main classes according to their physicochemical properties, as hydrophobic, cationic, amphipathic peptides (26,31,71). Hydrophobic CPPs are the least numerous sub-class, containing mainly peptides with nonpolar residues, which results in a low net charge (26,71). Despite being a poorly studied class, it's known that these hydrophobic motifs and their high affinity for hydrophobic domains are crucial for cellular internalization (71). It was even proposed that this group of peptides could spontaneously translocate, in an energy-independent manner, across membranes (72). The cationic class comprises peptides with a positive net charge at physiological pH, known to be essential for cellular uptake (71). Besides the overall high content of cationic AAs, specifically arginine and lysine, there is typically one or more non-polar amino acid, such as tryptophan present in the sequence that is important for high internalization efficiency (73,74). The importance of hydrophobic AAs has been previously shown using penetratin (Pen) as the model peptide. When the tryptophan in the 14^{th} position was replaced with phenylalanine, the peptide internalization into neuronal cultures was hampered (75).

Amphipathic CPPs can be divided into primary and secondary amphipathic peptides based on their sequence, length and association with lipids (26,76). The main difference is that the secondary amphipathic CPPs are not structured in solution, but upon membrane interaction, they adopt α-helix structure or a β-strand structure separating hydrophilic and hydrophobic residues in different sides of the amphipathic conformation (26,71,76). Changing the positions of tryptophan residues, like in case of PenetraMax (Pmax) represented in **Figure 1**, a Pen analogue, allows higher conformation flexibility and facilitates its insertion into the lipid bilayer (77,78). A balance between these properties are important to the biological function of a peptide, for example, cationic CPPs will preferentially interact with very anionic membranes, such as bacterial membranes, over eukaryotic membranes, which have an overall more neutral charge (34,48,79). Furthermore, the degree of interaction between the peptide and the membranes is differentiated by secondary propensities and by the amphipathicity of the peptide (80,81). These findings have prompted further investigations into possible antimicrobial properties of these peptides.

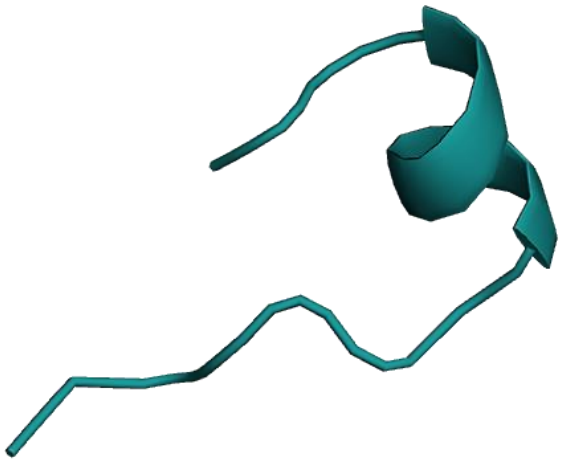

Figure 1 – The secondary structure of the CPP L-Penetramax. Created with PyMOL Molecular Graphics System with the structure provided the online database CPPsite 2.0 entry with ID 2127.

1.2.1.3. CPPs with antimicrobial properties

CPPs and AMPs share many key characteristics, namely, as described above, a strong positive net charge with a proportion of hydrophobic residues, a short length and a well-defined secondary structure while interacting with membranes. Due to these similar features, some CPPs and AMPs were investigated for antimicrobial and cell-penetrating properties, respectively (32,33). The shortage of new antibiotics has prompted the interest in AMPs, however, there is also huge potential for investigating CPPs due to their structural similarities with AMPs. Some examples of CPPs with antimicrobial properties are Pen, Tat_{48-60} (67,82), Pep-1 (83), pVEC (30,84) and TP10 (30). Most of this research will focus on determining the antimicrobial activity of some analogues of Pmax, therefore, this section will focus particularly on the antimicrobial properties of Pen's analogues (**Table 1**) (85–88). The variability of the Pen's MIC (minimal inhibitory concentration) could be explained by differences between strains, inter-laboratory differences and differences in environmental conditions, such as slight differences in media used, set-up conditions or incubation time/temperature (89).

Bahsen et al. reported a general tendency of higher antibacterial activity against Gram-negative over Gram-positive bacteria for most of the analogues studied. Furthermore, the researchers showed that a higher content of arginine enhanced the antibacterial effect, but the therapeutic index is less favourable, due to significantly higher cytotoxicity (85). These differences between lysine-rich and arginine-rich peptides have been well investigated, despite that, both are equally charged at physiological pH, the guanidium group of

arginine has the ability to function as a donor of two hydrogen bonds compared to the single-bond donation of lysine. This facilitates a stronger interaction between arginine and the membrane phospholipid or glycosaminoglycan (GAG) components (90,91). The substitution of methionine by leucine showed to reduce the risk of spontaneous oxidation of the peptide (92), but despite the similar antimicrobial activity, the cytotoxicity and hemolytic toxicity are slightly higher (85). Furthermore, the Nielsen group also compared the activity of L-Pen and D-Pen, which revealed that cell membrane integrity was more disrupted after exposure to the D-form (93). These results are consistent with the previous reports that showed an increased antimicrobial activity can be achieved by changing a peptide from L- to D- form (94).

Table 1 - Antimicrobial activity of Pen and its analogues *tested in Mueller Hinton Broth, **tested in Peptone broth and ***tested in other media towards [a] *E. coli* ATCC 25922, [b] *S. aureus* ATCC 33591, [c] *E. coli* 363, [d] *S. aureus*, [e] *E. coli* KCTC 1682, [f] *S. aureus* ATCC 29313, [g] *P. aeruginosa* KCTC 1637 and [h] *S. aureus* KCTC 1621.

Peptide abbreviation	**Sequence**	**MIC (μM)**		**Reference**
		Gram-negative	**Gram-positive**	
Pen	RQIKIWFQNRRMKWKK-NH_2	32 [a*]	64 [b*]	(85)
		>100 [c***]	>100 [d***]	(87)
		2 [e**]	28 [f*]	(86,88)
		4 [g*]	1 [h**]	(88)
PenLeu	RQIKIWFQNRRLKWKK-NH_2	32 [a*]	64 [b*]	(85)
PenArg	RQIRIWFQNRRMRWRR-NH_2	8 [a*]	16 [b*]	(85)
PenLys	KQIKIWFQNKKMKWKK-NH_2	64 [a*]	256 [b*]	(85)
Pen13	KIWFQNRRMKWKK-NH_2	128 [a*]	256 [b*]	(85)
Pen13Arg	RIWFQNRRMRWRR-NH_2	32 [a*]	32 [b*]	(85)
Pen13Lys	KIWFQNKKMKWKK-NH_2	256 [a*]	256 [b*]	(85)
Pen10	FQNRRMKWKK-NH_2	>256 [a*]	>256 [b*]	(85)
PenShuf	RWFKIQMQIRRWKNKK-NH_2	32 [a*]	64 [b*]	(85)
PenShufLeu	RWFKIQLQIRRWKNKK-NH_2	32 [a*]	16 [b*]	(85)
PenShufLysLeu	KWFKIQLQIKKWKNKK-NH_2	32 [a*]	32 [b*]	(85)
PenShufArgLeu	RWFRIQLQIRRWRNRR-NH_2	16 [a*]	16 [b*]	(85)

The CPP Pmax has been identified as the most promising Pen analogue due to its cell penetrating properties, however, the antimicrobial effects of this peptide were not evaluated. Kamei et al. and Khafagy et al. reported that Pmax, both L- and D- forms, greatly increase the intestinal and nasal absorption of insulin and without signs of inflammation, immunogenicity or toxicity *in vitro* and *in vivo* (95–99). Pmax, in L- and D-form, as well as lipidated versions of this peptide, are also currently being studied by the Nielsen group for their membrane disrupting and uptake enhancement properties (unpublished). Iwase et al. showed that D-Pmax can enhance the nasal absorption of IFN-β, reporting no damage to the epithelial membranes (100). The switching of the arginine residue on the N-terminus and lysine residue on the C-terminus can explain the significant improvement of the cell-penetrating properties. The specific AA position of both hydrophobic tryptophan residues could also play an important role to act as a carrier (101). Additionally, conjugation of a C10 lipid chain to Pmax significantly enhanced permeation of insulin across intestinal cells (102,103). Pmax seems to be an enhancement of the cell-penetrating properties of Pen (104) but the antimicrobial activity of this peptide as well as from its D-form and lipidated analogue is still unknown and will thus be evaluated in this project.

1.2.2. Nanocarriers for delivery of peptides

Despite the therapeutic potential and ongoing commercialization of peptides (105), there are still multiple challenges to overcome in order to allow their clinical use. The major obstacles are their chemical and physical instability (105–108). Chemically instability of peptides includes the formation or cleavage of covalent bonds, generating new chemical entities, via hydrolysis, oxidation, deamidation, racemization and among other chemical reactions. In the same way, physical instability refers to conformational changes, such as dimerization, which could result in denaturation, adsorption to surfaces, aggregation or precipitation (105,106). As a result of low stability, delivering peptide drugs to a specific therapeutic target is also hampered by its rapid renal clearance, short half-lives in the bloodstream, reticuloendothelial system recognition and off-target binding (106). For example, the infected tissue is often characterized by high proteolytic activity, mediated by both bacterial and human defence proteases, therefore resulting in a rapid peptide degradation and antimicrobial activity loss (109). A promising tool to overcome the restraints described above is the immobilization of these peptides into nanocarriers, a nanomaterial-based drug delivery system (**Figure 2**).

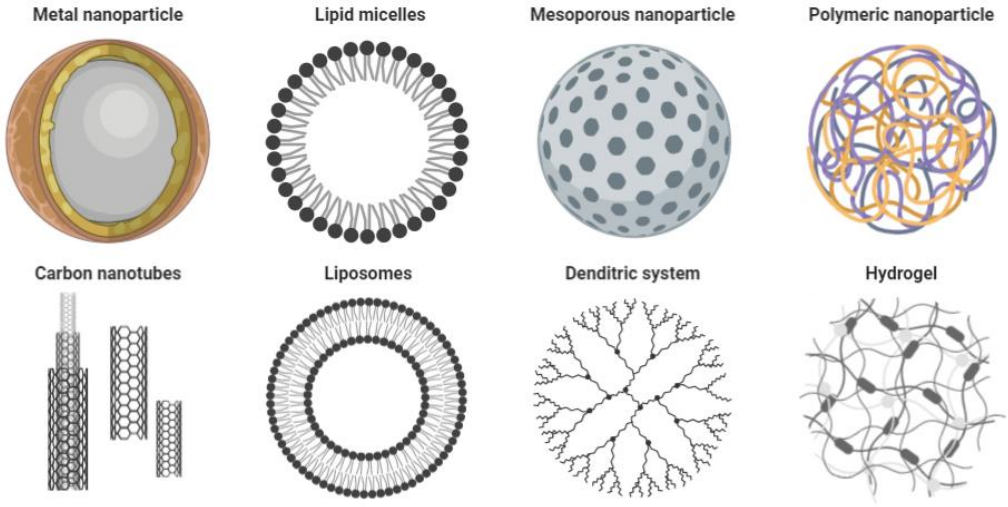

Figure 2 – Examples of nanomaterial-based drug delivery systems based on the results described in (19,40,109). Created with BioRender.com

Inorganic particles such as gold nanoparticles (AuNPs) were used as delivery systems of antimicrobial peptides. Alteriis et al. characterized the synthesis of AuNPs functionalized with the AMP indolicidin, a broad spectrum antibiotic (110). These conjugates, compared to the AuNPs and indolicidin alone, shown higher efficacy destroying biofilms formed by *Candida albicans* during *in vitro* experiments, possibly due to the fact that the peptide is protected from enzymatic degradation (110). Silver nanoparticles (AgNPs) are another example of metal nanoparticles used to deliver AMPs, which enable the combination of the antibacterial effect of silver with the effects of AMPs. Pal et al. described a higher antimicrobial activity of AgNPs functionalized with Andersonin-Y1, compared to the sum of the activities of the peptide and the nanoparticles taken individually, against the multidrug resistant strains *Klebsiella pneumoniae*, *P. aeruginosa*, and *Salmonella typhimurium* (111). Researchers have also tried to use carbon nanotubes (CNTs) for delivery of AMPs. Sur et al. that proved that indolicidin-CNTs conjugates could induce complementary innate immune gene activation and protect the host cells with a lower concentration than free peptide (112). Other promising inorganic nanocarriers are the silica nanoparticles (SiNPs), anionic mesoporous SiNPs have been employed to partially reduce proteolytic degradation of the loaded peptide LL-37 (113). However, positively charged mesoporous SiNPs can also cause hemolytic effects against human erythrocytes (113). Despite the therapeutic potential, inorganic nanoparticles have some drawbacks like metal toxicity, low degradability, expensive production as well as problems related to their stability and storage (114,115).

Soft polymeric nanoparticles, such as liposomes, nanogels or micelles suspended in a polymer matrix are also often used as nanocarriers for AMPs. Biodegradable polymers are particularly desirable for the encapsulation of AMPs, as their amphiphilic nature allows for a high drug loading (116). Loading AMPs into liposomes is a desirable strategy to prevent cytotoxicity associated with the direct use of AMPs as well as enhanced stability and bioactivity (117). Importantly, liposomes usually have to be coated with biocompatible polysaccharides (such as pectin, polygalacturonic acid and chitosan) or with polyethylene glycol to inhibit future aggregation and peptide release during storage, improving their stability (118,119). Pu et al. reported on the improved antibacterial and antibiofilm properties of chitosan-coated liposomes loaded with Apep10 towards *Listeria monocytogenes* (120). Liquid crystalline systems, such as cubosomes or hexosomes, have also been used to improve the AMP stability by reducing direct accessibility of proteolytic enzymes, but also resulted in decreased bactericidal activity (121,122).

Currently, (bio)polymeric nanoparticles have the greatest potential as carriers or agents for delivery of antimicrobial drugs due to their biocompatibility and biodegradability, their sustained release, chemical stability and their easy binding with the microbial cell wall (123). This is a class of nanocarriers that can be formed by an enormous diversity of polymers and consecutively a lot of interesting forms of matrices. Some of the most recent examples include polymers such as polylactic-co-glycolic acid (PLGA), polyethylene glycol (PEG), chitosan, hyaluronic acid, hyperbranched polyglycerol (HPG). These polymers are used extensively in drug delivery, where they function as drug carriers across the bacterial membrane, and when inside the cell membrane, they disintegrate and release the drug to its specific target site (124). Casciaro et al. developed PLGA nanoparticles to deliver esculentin-1a-derived AMP in cystic fibrosis patients presenting *P. aeruginosa* infection, and reported an improved vehiculation and antibacterial activity, both *in vitro* and *in vivo* (125). Almaaytah et al. studied the delivery of the RBRBR ultrashort AMP encapsulated into chitosan NPs, which proved to be able to reduce the toxicity of the free peptide and increased antibacterial activity (126).

Nanofibers are another kind of polymeric nanocarrier for AMPs' delivery. In the field of food safety applications, Soto et al. loaded the nisin cyclic AMP into amaranth protein isolate-pullulan (API-PUL) nanofibers, a formulation that proved to have bactericidal activity against *Salmonella typhimurium*, *Listeria monocytogenes*, and *Leuconostoc mesenteroides*, with a progressive release profile protecting nisin from degradation (127).

Finally, polymer-based hydrogels or nano-hydrogels (nanogels) are very promising as a drug delivery system because of their high loading capacity, high stability and responsiveness to micro-environmental

factors, such as pH, temperature and ionic strength. Additionally, the polymer functional groups can be easily modified with various targeting moieties to a specific delivery, allowing a stimuli-controlled release (128). Cleophas et al. investigated the design and synthesis of bactericidal PEG-based hydrogel coatings with covalently attached variants of HHC10 (H-KRWWKWIRW-NH2), an AMP develop for optimal stability in human serum while retaining strong antimicrobial activity against *S. aureus* and *S. epidermidis* (129). The final formulation proved to be a potent bactericidal while at the same time exhibited lower hemolytic toxicity. Water et al. studied the encapsulation of the AMP novicidin into an octenyl succinic anhydride-modified analogue of HA nanogel, with features that could be tuned by changing its preparation parameters (130). Nanogels revealed good stability with a maximum of 36% of peptide load, which was completely released after 14 days. Furthermore, the encapsulation of novicidin into HA-based nanogels decreased the toxicity of the free peptide against HUVEC and NIH 3T3 cells, without losing antimicrobial activity against *E. coli* and *S. aureus.* The excellent biocompatibility, biodegradation and non-immunogenic properties and its unique viscoelastic nature, explains why this polymer is a better choice for medical applications compared to synthetic polymers. HA has been used extensively over the years and drug delivery research (109,128,131) has resulted in many new HA-based carriers. The HA-based delivery systems developed for the delivery of AMPs are explored in the next section since HA will be the polymer base chosen to prepare a delivery system in this work.

1.2.2.1. Hyaluronic-based nanoparticles

HA is a naturally occurring glycosaminoglycan, a linear polysaccharide composed of repeating disaccharide units of D-glucuronic acid and N-acetyl D-glucosamine linked by β(1,4) and β(1,3) glucosidic bonds (132). As a natural polyanionic polysaccharide, biodegradable and biocompatible, this polymer represents an excellent starting material for the design of a delivery system (133,134). This polymer can also be easily modified to alter or enhance its properties, being extensively used for a range of medical applications. Due to its high negative net charge and hydrophilicity, it is excellent to encapsulate short cationic peptides (135). Additionally, delivery of AMPs using HA-based nanocarriers could result in a synergetic effect, although the HA antimicrobial activity is not clear. Ardizzoni et al. suggested a bacteriostatic effect of HA, but is highly dependent on its concentration and molecular weight as well as on the bacterial species (136).

As a hydrophilic polymer, HA does not self-assemble on its own and needs to be modified with hydrophobic moiety to assemble into a drug delivery system. It has been demonstrated that hydrophobized hyaluronan can form micelle-like structures (134,137). HA has a large number of reactive functional groups

that can be modified allowing a structural and functional diversity of HA-derivates. Although these HA-derivates may be significantly different from the native form, most maintain its biocompatibility and biodegradability (138).

Silva et al. developed a self-assembling HA-nanogel grafted with the hydrophobic 11-amino-1-undecanethiol, encapsulating the AMP LLKKK18 to investigate it as an anti-tuberculosis formulation (139). Peptide incorporation into the HA-nanogels was found to result in increased peptide stability and reduced cytotoxicity. Additionally, these nanogels were found to be effectively internalized by macrophages. This resulted in a significant reduction of the mycobacterial load in macrophages infected with either *Mycobacterium avium* or *Mycobacterium tuberculosis*. *In vivo*, intra-tracheal administration of the peptide-loaded nanogels reduced infection levels significantly, after just 5 or 10 every other day administrations. Nanogels composed of octenyl succinic anhydride-modified 50 kDa HA have previously been shown to improve antimicrobial activity of a peptide mimetic and reduce its cytotoxicity *in vitro* (140). It reduced, as well as, the *in vivo* toxicity of an antibiofilm peptide after subcutaneous and intravenous administration, without affecting the antibiofilm activity of the peptide (141). The same delivery system showed to reduce the toxicity of the peptide DJK-5, maintain its antimicrobial activity and provide an additional immunostimulatory effect (141). The release from these HA-based nanogels occurs within 5 h in a blood isosmotic medium (141) meaning it cannot be used for a sustained release of the peptide. Many researchers have also used cholesterol-modified HA (142,143) and many other different lipid chains (133,134,144) to develop self-assembling delivery systems with promising features.

Šmejkalová et al. proved that lipid-modified HA nanocarriers enhanced skin permeation of the loaded compounds into deeper epidermal and dermal layers (133). A lipid that has shown potential for antimicrobial activity effects as an absorption enhancer and synergistic effects with other delivery systems is oleic acid (145–148). The incorporation of this C18 lipid into HA-based polymeric micelles improved *in vitro* and *in vivo* bioactivity of the payload (133). Additionally, these micelles have shown to be stable after incorporation in cream preparations, representing a great potential for topical delivery systems (133). The incorporation of oleic acid into a delivery system has previously shown to result in fluidization of bacterial cell membrane and subsequently increase membrane permeability to the drug (146). As a result, this work will use the polymer oleic-grafted hyaluronan (OL-HA) to encapsulate the cell penetrating peptides.

1.2.2.2. Design considerations for antimicrobial application

There are important design considerations that should be taken into account when developing efficient nanocarriers. These include the physicochemical properties of the desired vehicles such as size, surface charge, hydrophobicity and shape. Other factors like encapsulation efficiency (EE) and release profile should be determined based on the intended route of administration and desired target activity. With the right characteristics, these nanocarriers offer an improved strategy to increase the therapeutic index, by decreasing the dosage and frequency of administration (19). Nanovehicles may also improve intracellular drug delivery and targeted organ accumulation, mitigating the development of drug-resistant bacteria and reducing systemic side effects and immunosuppression (4).

At infection sites, the release and accumulation of bacterial components are known to trigger multiple inflammatory mediators that increase vascular permeability (149,150). The features of bacterial infections make passive size-mediated targeting possible, due to the enhanced permeation and retention (EPR) effect, similar to what happens in solid tumour tissue (151). Additionally, the impaired lymphatic drainage system has also been reported in bacterial infections, which can contribute to nanoparticle accumulation at the infection sites (152). Size is one of the key features, usually the nanoparticles have to be smaller than 600 nm to favoured by the EPR effect and bigger than 10 nm to avoid extravasation into healthy tissues (153,154). In general, the transport across the vasodilated vessels increases with the decreasing of the nanoparticle size, however, it has to be large enough to ensure retention at the infection site. Considering an intravenous administration route, the nanoparticle size should be smaller than 200 nm to avoid its clearance from the bloodstream and accumulation in the liver and spleen (155,156). Additionally, deformable particles such as micelles or nanogels are more desirable than solid ones due to their ability to extravasate into infected tissue (157). Another important feature is the nanoparticle surface charge. Although cationic nanoparticles can improve bacterial targeting due to their electrostatic interactions with the anionic surface charge of bacteria (152), the cationic charge is also associated with increased toxicity towards mammalian cells and binding to serum proteins, which effectively disables the peptide or particle activity. As a result, anionic nanoparticles are more desirable as they have shown to reduce local inflammation (158) and are associated with lower toxicity compared to cationic particles (159). Finally, in order to eradicate bacterial infections efficiently, fast release from the nanocarrier is desirable, as it will expose the bacteria to high peptide concentrations allowing efficient bacterial eradication. In contrast, a slow and controlled release may contribute to AMR by exposing the bacteria to very low antimicrobial concentrations.

2. Hypothesis and aims

It is hypothesized that the CPPs Pmax, both L- and D- form and also a lipidified form (Syn 2) can in fact possess antimicrobial activity, and that can be encapsulated into HA-based micelles in order to minimize their toxicity and improve their therapeutic effect.

Aim 1: Develop and optimize the formation of anionic, hydrophilic polymer micelles of <200 nm prepared using OL-HA for encapsulation and fast release of the abovementioned CPPs.

Aim 2: Evaluate the physiochemical characteristics of the micelles: diameter, zeta potential (ZP), morphology, encapsulation efficiency and release profile.

Aim 3: Assess the cytotoxicity and the antimicrobial activity of the abovementioned CPPs and loaded micelles against *Escherichia coli*, *S. aureus* and *P. aeruginosa*, three of the most dangerous ESKAPE pathogens.

3. Materials and methods

3.1. Materials

Sodium oleyl hyaluronate (5-20 kDa, 5-15% degree of substitution) was purchased from Contipro (Dolní Dobrouč, Czech Republic). Standard salts and buffers, Mueller-Hinton broth (MHB), Dulbecco's Modified Eagles Medium (DMEM), crystal violet, were obtained from Sigma-Aldrich (St. Louis, MO, USA). L-Pmax (KWFKIQMQIRRWKNKR), D-Pmax (kwfkiqmqirrwknkr) and Syn 2 (KWFK(capric acid)IQMQIRRWKNKR) were synthesized and purified to >95% by Synpeptide (Shanghai, China) and stored lyophilized until use. Analytical grade solvents for HPLC analysis were purchased from Merck (Darmstadt, Germany). Horse red blood cells (RBC) were provided by Statens Serum Institut, Copenhagen, Denmark. Ultrapure water for sample preparation or analysis was obtained from a PURELAB® flex 4 (ELGA LabWater, High Wycombe, UK). *E. coli* ATCC 25922, *P. aeruginosa* PA01 (reference strain) and *S. aureus* 15981 (clinical isolate strain) were provided by the Institute of Immunology and Microbiology, University of Copenhagen.

3.2. Preparation of the polymeric micelles

3.2.1. Solvent evaporation method

The micelles were formed by preparing an emulsion with a ratio of aqueous phase to organic phase of 1:1, as described before (137). The aqueous phase was prepared by mixing the same volume of the polymer OL-HA solution (2 mg/mL) and the peptide solution in different concentrations (200, 600 and 1000 µg/mL). Subsequently, 2-propanol (2-PrOH) at 100% was added as the organic phase. The final emulsion was then vortexed at approximately 400 rpm and placed on a rotary evaporator (Laborota 4011 digital, Heidolph, Schwabach, Germany) at 40 rpm until the glass flasks were completely dried at room temperature. The thin film was then rehydrated with ultrapure water, the same volume as the initial aqueous phase, for approximately 1 h on the rotary evaporator (with the vacuum pump turned off) at 80 rpm.

3.2.2. Probe-sonication method

First a 1:1 aqueous phase: organic phase emulsion was prepared as described previously. The emulsion was vortexed and sonicated using a Missonix S-4000 ultrasonic sonicator for 5 min (3 s on and 2 s off) with an amplitude of 60%. The temperature was controlled using ice. The solution was then left evaporating in the fume hood with agitation, and samples were taken out after 60, 90 and 120 min. An

independent replicate was also left to evaporate overnight and another evaporated using the rotary evaporator, as controls to ensure complete evaporation. The samples were also rehydrated before the Zetasizer measurements.

3.2.3. Microfluidic method

The polymeric micelles were also produced by microfluidics assisted self-assembly, using a previously described microfluidic chip design (160), which were stored at room temperature before use. OL-HA and peptide aqueous solutions were loaded in three syringes (Hamilton, Reno, NV, USA) and mounted on two 11 Elite syringe pumps (Harvard Apparatus, Holliston, MA, USA) to control the flow rates. The peptide solution was injected into the centre stream of the microfluidic chip and the polymer solution into the outer streams (9:1 v/v). To prepare empty OL-HA micelles the peptide solution was replaced by ultrapure water. This setup is outlined in **Figure 3**. The initial polymer concentration used was 1.1 mg/mL (in ultrapure water or 2-PrOH) and the peptidomimetic to polymer ratio was 0.1 and 0.3, tested at the low (2.2 mL/min) or high (11 mL/min) flow rate according to the parameters previously tested (140). The experiment was performed at room temperature and 4 °C. The samples containing 2-PrOH were measured before and after evaporation using the Zetasizer.

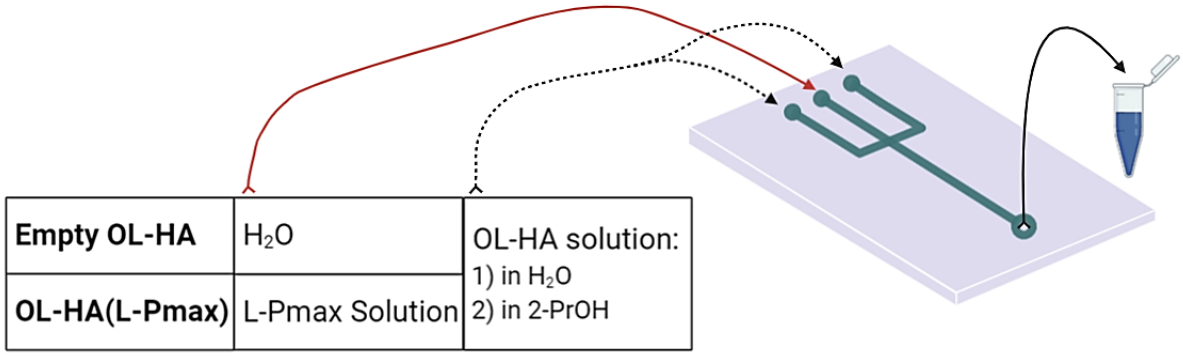

Figure 3 – Microfluidic setup for micelles preparation. The schematics show the channels available in the microfluidic system as well as the solutions utilized in each of the channels. Created with BioRender.com

3.3. Size and Zeta potential measurements

The average micelles size and polydispersity index (PDI) were obtained by dynamic light scattering (DLS) and micelles zeta potential (mV) was calculated by electrophoretic mobility. These measurements were performed at 25 °C in miliQ water and with an angle of 173° using a Zetasizer Nano ZS (Malvern Instruments, Worcestershire, UK) equipped with a laser beam at a wavelength of 633 nm. The data were acquired and analysed using Malvern Zetasizer software version 7.12.

3.4. Polymeric micelles imaging

The polymeric micelles were visualized using transmission electron microscopy (TEM) by negatively staining with uranyl acetate. A carbon-coated grid was glow discharged, after which 3 µL of nanoparticle dispersion was deposited on the surface. After air drying it for 1 min, 3 µL of 0.5% w/v uranyl acetate solution was added, 2 min after the grid was rinsed once and blotted with filter paper. Afterwards, samples were visualized using a CM100 (a) TWIN microscope (Philips/FEI, Hillsboro, OR, USA). The size of the micelles was measured using Image J software (161).

3.5. Peptides encapsulation efficiency

To determine the encapsulation efficiency (EE) of the peptides in OL-HA micelles, the amount of residual peptide in the aqueous bulk phase after particle production was measured. The micelles dispersions (200 µL) were centrifuged at 500 000 g for 30 min to obtain a particle-free supernatant (50 µL). Quantification of EE was performed three times as triplicates on three separate days. Calculations of EE are based on the total amount of peptide used to prepare each batch (**Equation 1**).

$$\mathrm{EE\%} = \frac{\text{Theoretical conc.}\frac{\mu g}{mL} - \text{Measured conc.}\frac{\mu g}{mL}}{\text{Theoretical conc.}\frac{\mu g}{mL}} \times 100\% \qquad \textbf{(1)}$$

3.6. Peptides release from polymeric micelles

The release studies were performed in HEPES buffer (10 mM, pH 7.4) with the ionic strength adjusted to 150 mM NaCl. Briefly, the polymeric micelles were diluted in miliQ water, added to a dialysis device (Spectra-Por® Float-a-Lyzer® G2, MWCO 100 kDa, Spectrum Labs, Breda, the Netherlands) and placed in the release buffer, with stirring at 225 rpm, approximately. The temperature was maintained at 37 °C in an incubator throughout the 96 h of the assay. At each time point, 50 µL were withdrawn from the outside of the membrane and replaced with release buffer, maintaining sink conditions. The cumulative peptide release (%) was calculated according to **Equation 2**, where V_e is the volume release media removed each time point, V_0 is the total volume of the release media (19 mL), C_i is the peptide concentration in the release media and m_0 is the total peptide amount.

$$\text{Cumulative peptide release (\%)} = \frac{V_e \sum_1^{n-1} C_i \; + \; V_0 C_n}{m_0} \times 100\% \qquad \textbf{(2)}$$

3.7. Peptides quantification

Peptide concentrations were quantified using reverse phase high performance liquid chromatography (HPLC) on a Shimadzu Prominence HPLC system (Kyoto, Japan) using a Kinetex XB-C18 column, (50 × 2.1 mm, 2.6 µm, Phenomenex, Torrance, CA, USA) measuring the absorbance at 218 nm. The mobile phase consisted of eluent A [95% (v/v) acetonitrile: water] and eluent B [5:95% (v/v) acetonitrile: water], both containing 0.1% (v/v) TFA. Samples were run with a gradient of 0 ⟶ 80% eluent B over 13.50 min at 0.8 mL/min at 40 °C. A calibration curve was performed beforehand.

3.8. Cellular viability

Cellular cytotoxicity was determined by using the MTS/PMS assay. HepG2 cell line was cultured in treated flat-bottomed 96-well MicroWell™ plates (NUNC, Roskilde, Denmark) at a seeding density of 3 x 10^5 cells/well under standard culturing conditions (37 °C, 5% CO_2, humidified air). DMEM supplemented with penicillin (100 U/mL), streptomycin (100 µg/mL), L-glutamine (2 mM), sodium pyruvate (1 mM), non-essential amino acids (1% v/v), and FBS (10% v/v) was used. HUVEC and Caco-2 cell lines were cultured in

collagen-coated flat-bottomed 96-well MicroWell™ plates (NUNC, Roskilde, Denmark) at a seeding density of 3 x 10^5 cells/well in DMEM supplemented with penicillin (100 U/mL), streptomycin (100 µg/mL), L-glutamine (2 mM), non-essential amino acids (1% v/v), and FBS (10% v/v) under standard culturing conditions (37 °C, 5% CO_2, humidified air).

The cells were grown until confluency of 80-90% before use. On the day of the experiment, cells were washed twice with Hanks Balanced Salt Solution (HBSS) (Gibco, Paisley, UK), supplemented with 10% (w/v) HEPES (AppliChem, Darmstadt, Germany), the buffer that was also used throughout the assay. The free peptides and the loaded micelles were diluted in HEPES-HBSS with a peptide concentration range 10 – 300 µg/mL and immediately applied to the cells and incubated for 3 h at 37 °C and 50 rpm. The HEPES-HBSS buffer was used as a negative control, defined as 0% cell death (Abs_{neg}), while 0.2% of Sodium dodecyl sulfate (SDS) in HEPES-HBSS was used as the positive control, defined as 100% cell death (Abs_{pos}). The solutions were removed after the incubation period, the cells were washed twice with HEPES-HBSS and 100 µL of MTS/PMS in HEPES-HBSS (240 µg/mL MTS to 2.40 µg/mL PMS) was applied to the cells. The cells were further incubated (37 °C, 50 rpm) until an absorbance of approximately 0.5 for the negative controls was reached.

Absorbance was measured on a microplate reader (FLUOstar Omega, BMG Labtech, Ortenberg, Germany) at 492 nm. Tests were performed in triplicates on two different passages. The relative viability was calculated according to (**Equation 3**):

$$\text{Viability } (\%) = \frac{\text{Abs}_{\text{sample}} - \text{Abs}_{\text{pos}}}{\text{Abs}_{\text{neg}} - \text{Abs}_{\text{pos}}} \times 100\% \qquad \textbf{(3)}$$

3.9. Hemolytic effect

The lysis of RBCs was determined to evaluate the toxicity of the particles towards erythrocyte. Briefly, horse RBCs (Statens Serum Institut, Copenhagen, Denmark) were washed twice with 10 mM HEPES-HBSS pH 7.4 followed by centrifugation at 5 000 g for 5 min. Two-fold serial dilutions of the free peptides or peptide-loaded micelles in HEPES-HBSS were added to each well in a flat-bottom 96-well plate (Nunc, Thermo Scientific, NY, USA).

A 1% (v/v) RBC suspension in HEPES-HBSS was added to each well to reach a total volume of 100 µL in each well, obtaining final peptide concentration range 5 – 400 µg/mL. The plate was incubated for 1 h at 37 °C, and then the supernatant was transferred to a second well-plate (flat bottom polystyrene 96-well plate (Nunc, Thermo Scientific)) to measure the absorbance of the released haemoglobin at 414 nm on the plate reader (FLUOstar Omega). The absorbance after incubation of the cells with 0.2% SDS defined 100% hemolysis (Abs_{pos}) and the cells incubated with HEPES-HBSS defined 0% hemolysis (Abs_{neg}). The hemolysis was calculated according to (**Equation 4**).

$$\text{Hemolysis (\%)} = \frac{\text{Abs}_{\text{sample}} - \text{Abs}_{\text{neg}}}{\text{Abs}_{\text{pos}} - \text{Abs}_{\text{neg}}} \times 100\% \quad \textbf{(4)}$$

3.10. Antibacterial activity

Bacterial growth inhibition of the peptides and peptide-loaded micelles was determined using broth microdilution, according to Clinical Laboratory Standards Institute guidelines (162). Solutions of the peptides and the peptide-loaded micelles were prepared in two-fold dilutions in the concentration range of 128 – 1 µg/mL in MHB. 100 µL of each sample was placed in separate wells of a 96-well polypropylene round bottom plate (Costar Corning®, Vordingborg, Denmark) and inoculated with *E. coli*, *S. aureus* or *P. aeruginosa* in log phase to yield a final bacterial concentration of 2 - 5 x 10^5 CFU/mL. The inoculated plates were incubated statically for 20 h at 37 °C in ambient air before visual inspection of growth. The MIC values were determined as the lowest concentration showing no visible bacterial growth. This assay was performed as two biological replicates (three technical replicates) on two different days.

For assessment of biofilm prevention activity, peptide and peptide-loaded micelles solutions were tested as previously described (163). Briefly, 100 µL of each concentration was placed into separate wells of a 96-well polypropylene round-bottomed plate. The wells were then inoculated with *P. aeruginosa* to yield a final concentration of 2-5×10^5 CFU/mL and incubated statically at 37 °C for 20 h. To quantify the formed bacterial biofilm, the contents of each well were removed and the wells were washed with pre-warmed (37 °C) PBS to remove non-adherent bacteria. The remaining biofilm was stained with 100 µL of the aqueous solution of crystal violet (1 mg/mL) for 5 min, after which the plates were washed twice with pre-warmed PBS. The cell-bound crystal violet was dissolved by adding 200 µL of 96% ethanol to each well, and the

absorbance was measured using a POLARstar Optima spectrophotometer (GMBLabtech, Offenburg, Germany) at 540 nm. Bacteria grown in absence of peptides or peptide-loaded micelles were used as growth control. The growth control wells were stained with crystal violet and their absorbance was taken as 100%. Experiments were performed at least as two biological replicates (three technical replicates each) on two different days.

3.11. Statistical analysis

For the particle optimization, one replicate was performed for each condition, due to time limitations, except if, is differently indicated. For the particle characterization, three replicates or more were performed. For *in vitro* experiments, three independent experiments were conducted and are presented as mean ± standard deviation (SD). For each graph, the number of technical replicates is indicated by N and mean ± SD where relevant. Statistical evaluations and data modelling of *in vitro* experiments were performed using GraphPad Prism 8.4.2 (GraphPad Software, La Jolla, CA, USA). One-way analysis of variance (ANOVA) with Dunnett's post-test was carried out to compare the means of different data sets within the loaded micelles characterization experiments. A value of $p < 0.05$ was considered statistically significant.

4. Results and discussion

This project consisted of two main parts: establishment and optimization of the preparation method for the formation of small OL-HA micelles capable of encapsulating the peptides, followed by evaluation of the physicochemical properties and *in vitro* performance of the formed delivery system. The result section has been divided accordingly.

4.1. Establishment and optimization of the preparation method for formation of OL-HA micelles

The preparation method for the formation of the OL-HA based particles was based on the available literature, in which the particles were prepared by solvent evaporation using 2-PrOH. This method has previously resulted in spherical micelles, loaded with paclitaxel with about 70 (wt.%) loading efficiency, with a size range of approximately 60 – 80 nm, determined by Cryo-SEM (137). However, when measured by DLS, the micelles presented a fully hydrated size almost 10 times larger (137). Another study used chloroform instead of 2-PrOH for the preparation of these particles, and the hydrodynamic diameter of the loaded nanoparticles was approximately 200 nm (133). The use of chloroform was disregarded for this study due to possible residual solvent contamination in the sample that could result in toxicity (164). Additionally, this first part aim is to optimize and establish the particles preparation method to obtain the desired particle size (<200 nm) to be administrated intravenously.

4.1.1. Evaluation of emulsion mixing method

Particles composed of OL-HA were initially prepared using the solvent evaporation method as previously described, with a starting polymer concentration of 10 mg/mL and using 2-PrOH as the organic solvent. A range of solvent to drug/polymer solution ratios were evaluated to establish the most appropriate ratio for the formation of small particles. Additionally, the influence of the emulsion mixing method on the formation of particles was assessed by comparing two methods, namely vortexing and magnetic stirring. The findings on obtained particle hydrodynamic diameters and PDIs are summarized in **Figure 4**. The results showed that the particle z-average and PDI slightly decrease when increasing amounts of 2-PrOH and vortexing are using for particle formation. This effect is more preeminent in the PDI values than in the z-average. Overall,

the PDI is higher when the emulsions are mixed using magnetic stirring. As a result, vortexing was chosen as the emulsion mixing method for the following experiments. Both mixing methods resulted in micelles with smaller hydrodynamic sizes than those reported in the literature (137), which could be due to the lower measured concentrations or the loaded content.

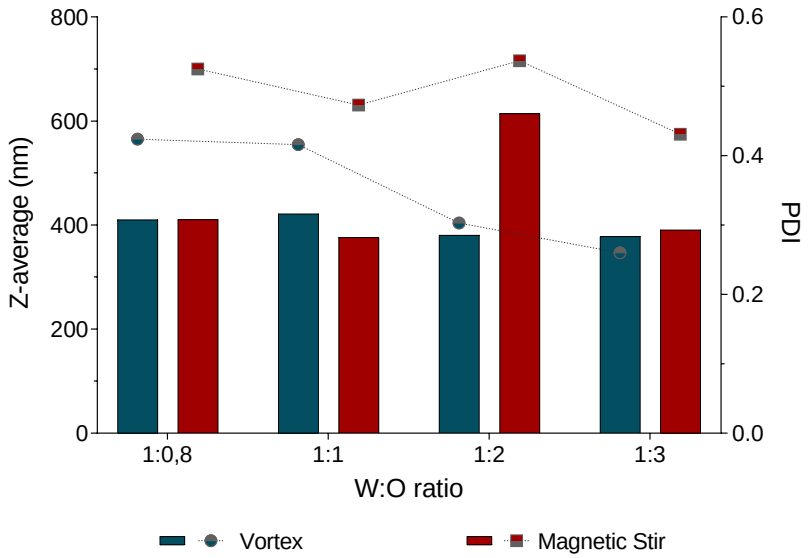

Figure 4 – Influence of solvent ratio and emulsion mixing method on particle Z-average (nm) and PDI. Z-average is illustrated in form of bars whereas the PDI is shown as points connected with a dotted line. Two mixing methods were utilized: Vortex (blue) and Magnetic stirring (red). N=1.

The role of emulsion mixing method or the ratio of aqueous phase to organic solvent on particle diameter and PDI needs further investigation. Nešporová et al. reported the encapsulation of curcumin into OL-HA micelles using magnetic stirring at an unspecified speed to mix the emulsion, which resulted in a bimodal size distribution with a diameter around 15 – 50 nm and 200 – 300 nm (134). However, the filtration of the polymeric nanoparticle suspension could explain why smaller micelles were obtained.

4.1.2. Determination of the polymer concentration

In an attempt to reveal the polymer concentration most suitable for the preparation of these particles, the micelles suspension was diluted and the particle size at various concentrations was measured (**Figure 5**). The results showed that decreasing the polymer concentration from 10 mg/mL to 1 mg/mL decreases the size of the formed polymeric micelles from 400 nm to approximately 200 nm. Although the ratio of solvent

to water phase used did not affect the particle size at various concentrations, it did have an effect on the PDI of the formed particles. The 2:3 ratio showed substantially higher PDI than the 1:3 ratio, independent of polymer concentration. As particles at 1 mg/mL polymer resulted in the smallest particle size, the polymer concentration for particle preparation was set to 1 mg/mL.

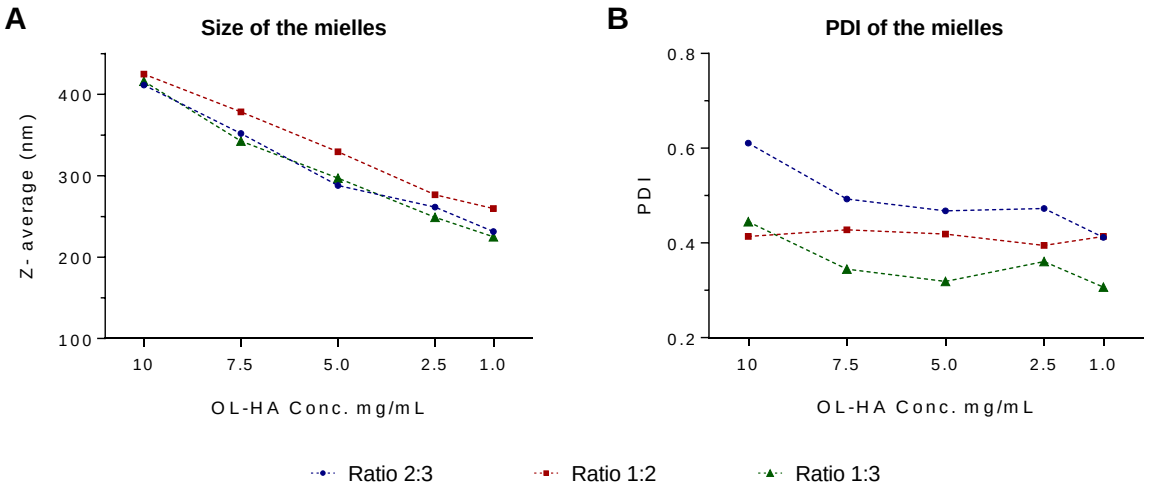

Figure 5 – Influence of OL-HA concentration (mg/mL) and solvent to water ratio on particle (A) Z-average (nm) and (B) PDI. N=1

4.1.3. Determination of solvent to water phase ratio

In order to evaluate the effect of solvent to water phase ratio in more detail, particles were prepared using 10 mg/mL and 1 mg/mL of polymer and various ratios of organic to water phase mixing the emulsion by vortex. 10 mg/mL concentration was used for comparison purposes. Results showed that using different polymer concentration and solvent ratios has an opposite effect on the size of the micelles (**Figure 6**). While using 10 mg/mL OL-HA with increasing amounts of 2-PrOH in the emulsion ratio resulted in a decrease in particle size, the opposite was observed when particles were formed using 1 mg/mL OL-HA. The ratio of aqueous phase to organic phase chosen to proceed with the optimization was 1:1 since it is the ratio with the best compromise between the size of the micelles and the PDI.

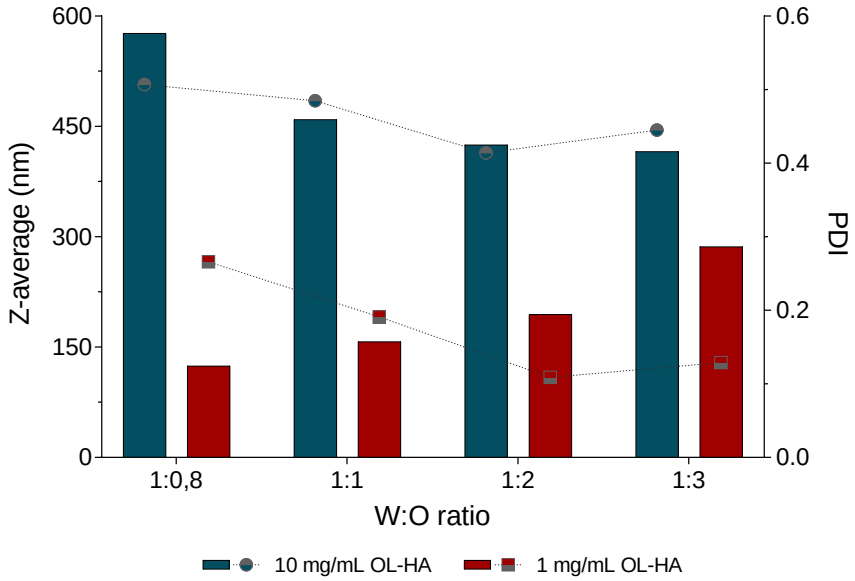

Figure 6 – Influence of solvent ratio and polymer concentration on particle Z-average (nm) and PDI. Z-average is illustrated in form of bars whereas the PDI is shown as points connected with a dotted line. N=1

HA is a hygroscopic polymer that possesses a high capacity for water retention (165), which could possibly explain the larger hydrodynamic sizes of the micelles made at higher polymer concentrations (166,167). The polymer solubilization time was also evaluated but results showed that it is not a relevant parameter to the diameter or PDI of the micelles (data not shown).

4.1.4. Evaluation of probe sonication method and solvent evaporation methods for particle preparation

Sonication is commonly used for dispersion of nanomaterials in aqueous media, improving homogeneity, suspension stability and decreasing nanoparticles diameter (168–170). A probe-sonication method was used to improve the size results obtained with solvent evaporation method and was followed by evaporating the emulsion in the fume hood with magnetic stirring instead of using the rotary evaporator. Various evaporation times were evaluated to determine the influence of this factor on the size of the micelles and PDI. The micelles size decreased almost 600 nm when the evaporation time was increased by one hour, from 60 min to 120 min (**Figure 7**), but the size did not change in comparison to when the samples were left to evaporate overnight. The samples left to evaporate overnight resulted in complete evaporation and formation of a thin film which required rehydration with ultrapure water. Additionally, leaving open vials in a

fume hood overnight may result in some contaminations during evaporation. The excessive heat generated by the sonication probe tip may have caused chemical degradation (171) of both the polymer and peptide, which can explain the high PDI values. Using this method the evaporation over 120 min is the best option.

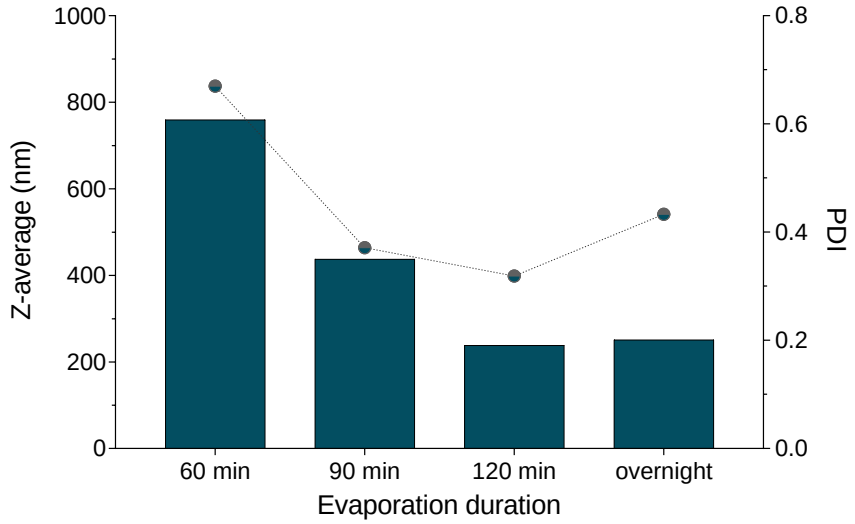

Figure 7 – Influence of the evaporation time on particle Z-average (nm) and PDI. Z-average is illustrated in form of bars whereas the PDI is shown as points connected with a dotted line. N=1

Subsequently, the production method with evaporation with magnetic stirring (in the fume hood) was compared to evaporation on the rotary evaporator. Combining the sonication technique with the evaporation on the rotary evaporator (by vacuum) slightly improved the results in comparison to evaporation in the fume hood, from a z-average of approximately 250 nm to 215 nm and a PDI of 0.4 to 0.3. However, the combination of these methods still resulted in particles larger and more polydisperse than if the rotary evaporation method alone was used. As a result, this method was determined to be better than sonication combined with evaporation in the fume hood or sonication combined with evaporation using a rotary evaporator (**Figure 8**).

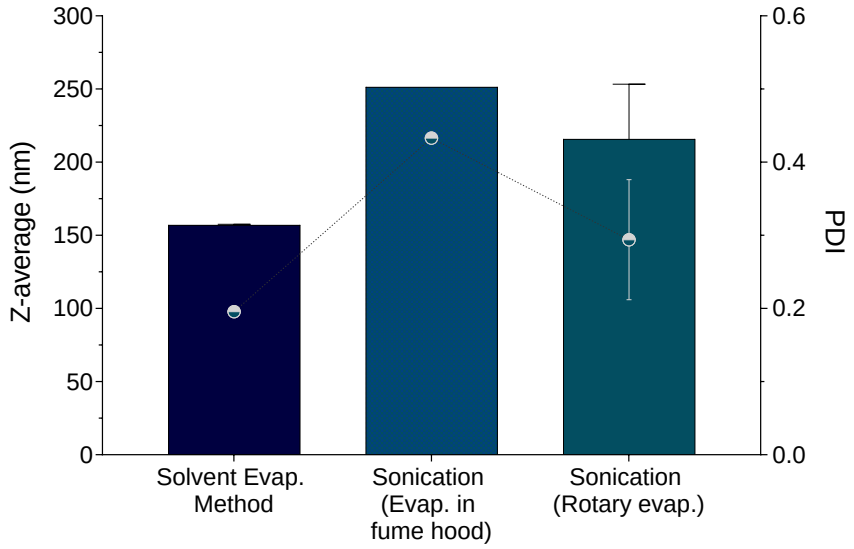

Figure 8 – Comparison between different polymeric preparation methods: Z-average (nm) is illustrated in form of bars whereas the PDI is shown as points connected with a dotted line. Solvent evap. method (N=1) refers to the procedure previously described; Sonication (evap. in fume hood) (N=1) describes the addition of a sonication step to the previously described method followed by evaporation in the fume hood; and Sonication (rotary evap.) (N=2) refers to the procedure with an extra sonication step followed by evaporation in the rotary evaporator.

4.1.5. Evaluation of microfluidics-assisted self-assembly for particle preparation

The microfluidic microchannels can provide dynamic control over the flow and the mixing that can be manipulated to optimize the characteristics of the nanoparticles, due to a continues formation process (172–174). These controlled conditions can lead to more homogeneously nano-sized particles and avoid self-aggregation (173). Bicudo and Santana described the synthesis of HA nanoparticles cross-linked with adipic dihydrazide and chloride carbodiimide by nanoprecipitation at the interface of organic solvent/ water phases using microfluidics methodologies, with sizes ranging from 140 to 460 nm (175). This method has also been used by Klodzinska et al. to form monodisperse HA-based nanogels for delivery of azithromycin (176) and the peptidomimetic LBP-3 (140).

As the polymer used in this project is an amphiphilic derivative of HA with potential to self-assemble, the optimization of the micelles preparation also included microfluidics assisted self-assembly method in various conditions in order to evaluate whether it is possible to prepare smaller and monodisperse micelles without the use of organic solvents. The particles were prepared at room temperature (≈ 25 °C), in ultrapure

water or a 50% solution of 2-PrOH in water and at two different flow rates. The particles solutions prepared in 2-PrOH were measured before and after evaporation. The results are presented in **Figure 9**. Higher flow rates showed bigger micelles size and higher PDI values. On a second instance, it seems that 2-PrOH only makes a difference at the lowest flow rate, since after evaporation the size decreases. At lower temperatures, the particle suspension was more polydisperse and with bigger sizes (data not shown).

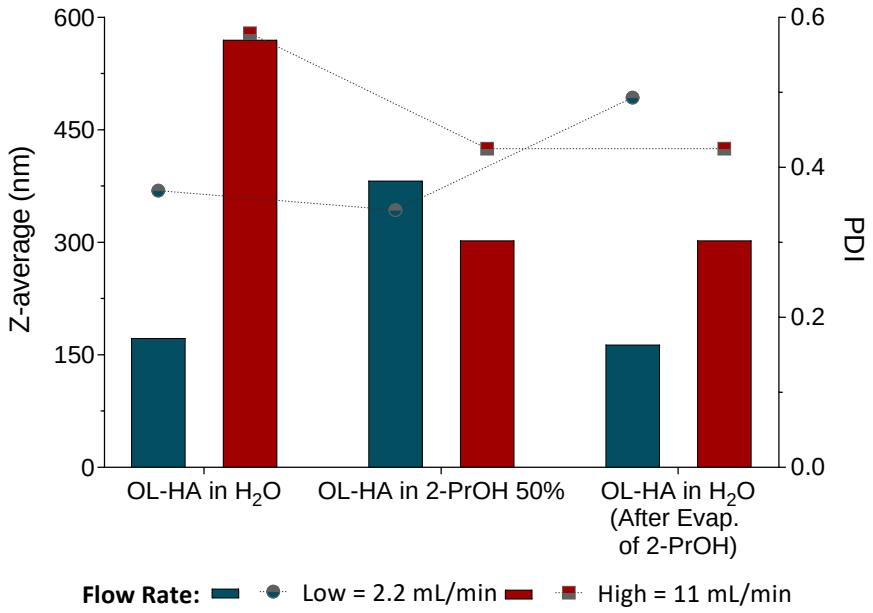

Figure 9 – Influence of the microfluidic flow rate and the dispersion solvent of the polymeric suspension. Z-average (nm) is illustrated in form of bars whereas the PDI is shown as points connected with a dotted line. OL-HA in H2O (after Evap. Of 2-PrOH) describes the size and PDI of the micelles obtained after evaporation of 2-propanol followed by rehydration with H2O. N=1

This method was also used to encapsulate L-Pmax but resulted in very low encapsulation efficiency and some white precipitate was visible within the microchannels, which could indicate that the peptide is sticking to the microfluidic chip material (177).

4.1.6. Determination of the ratio peptide to polymer

Based on the previous results, the solvent evaporation method was used to load the L-Pmax into the micelles, with the comparison of different ratios to optimize the formulation and to achieve the highest encapsulated amount of peptide in well-defined micelles (**Table 2**). Here, L-Pmax was chosen as a model peptide for the encapsulation assays.

The highest ratio of L-Pmax to OL-HA showed the highest amount of encapsulated peptide (94.3% ± 1.1). However, it was observed some particle precipitation in the suspension, indicating that this value could be the result of the particle aggregation and sedimentation and not the actual peptide encapsulation (**Figure 18,** section "***Appendix***"). This proposed explanation is also supported by the fact that the ZP of this suspension is less negative than the empty micelles and other formulations, likely due to a large amount of cationic peptide present. The 0.3 ratio was the ratio chosen to continue with the studies since it has the best characteristics to be used in drug delivery, smaller sizes, lower PDI and higher encapsulation efficiency.

This ratio was also tested with a slightly different method: first preparing empty micelles and then use a peptide solution in ultrapure water to rehydrate the thin film, followed by encapsulation of the peptide after the formation of the particles. Unfortunately, this method has a substantially lower encapsulation efficiency, larger sizes and higher PDI, likely due to the presence of empty micelles as well as loaded micelles. For those reasons, we discarded this methodology for future tests.

Table 2 – Influence of the different peptide to polymer ratios on the formation of empty and L-Pmax-loaded micelles The assessed parameters include Z-average (nm), size (nm) by number distribution, PDI, zeta potential (ZP) and percentage of encapsulation efficiency (EE%). *Different method of preparation: peptide encapsulation after preparing empty micelles.

	Peptide/Polymer ratio	**Z-average (nm)**	**Size (nm)**	**PDI**	**ZP (mV)**	**EE%**	**N**
Empty OL-HA	0	190.6 ± 28.1	126.2 ± 33.3	0.23 ± 0.09	-50.68 ± 2.30	–	8
OL-HA1	0.1	325.2 ± 27.8	246.9 ± 19.0	0.25 ± 0.03	-48.45 ± 2.67	60.9 ± 0.5	2-4
OL-HA3	0.3	235.5 ± 44.4	165.8 ± 47.0	0.19 ± 0.02	-46.78 ± 1.18	78.7 ± 11.7	7-12
OL-HA3*	0.3	365.9 ± 41.8	148.2 ± 25.9	0.47 ± 0.11	-44.50 ± 1.20	49.7 ± 7.5	5
OL-HA5	0.5	254.9 ± 95.7	144.2 ± 55.0	0.29 ± 0.08	-39.15 ± 1.75	94.3 ± 1.1	2-5

The method for preparation of the micelles was optimized according to the results obtained for the empty OL-HA micelles. It was determined that the solvent evaporation method was the best option among the methods tried, using vortexing to mix the emulsion with a 1:1 solvent to water phase ratio and a polymer concentration of 1 mg/mL. With the optimized procedure of micelles formation, it was possible to achieve the main goal of this first part of the project: small, anionic micelles capable of efficiently loading CPPs to tackle possible bacterial infections.

4.2. Evaluation of the physicochemical properties and in vitro performance of the formed particles

4.2.1. Physicochemical characteristics of the micelles

The formulations encapsulating the peptides L-Pmax, D-Pmax and Syn 2, as well as non-loaded formulations, were prepared using the solvent method with the parameters previously optimized and established in part 1 of the project. The size of the particles was first measured using dynamic light scattering (DLS) and are presented as both z-average and size by number distribution (**Figure 10 A**). Particle size can be affected by numerous factors such as solution pH, ionic strength and viscosity, the thickness of the solvation shell and by extension the size is also influenced by all substances adsorbed on the surface of the micelles (178,179).

The DLS technique is a very practical technique and recommended for size measurements in aqueous conditions, since it considers the particle diffusion, although it is still not completely representative of an *in vivo* situation (179,180). During administration *in vivo* and independently on the chosen route, the particles may suffer alterations, for example, due to opsonization by serum proteins the particle diameter can increase (154,181). The z-average size and the PDI are obtained from the cumulants analysis, calculated from the intensity signal (182). However, detailed distribution size analysis of the results is recommended when the sample is not monodisperse, indicated by a PDI above 0.1 (182). The intensity of scattering of a particle is proportional to the sixth power of particle diameter, which means that larger particles scatter much more light underestimating the proportion of the smallest particles (178,183). The corresponding number distribution provides a mean size associated with the relative percentage of particles in each size class (182).

The z-average of the micelles loaded with the L- and D- form is 235.5 ± 44.4 nm and 240.3 ± 56.4 nm, respectively. The mean size based on the number of particles of the particles loaded with the L- and D-

form is 165.8 ± 47.0 nm and 165.9 ± 29.6 nm. Despite the L-Pmax and D-Pmax micelles size being very similar, the encapsulation efficiency is somehow different: 79% ± 12 (N=7) and 63% ± 12 (N=5) for L-Pmax and D-Pmax, respectively. As expected, micelles encapsulating Syn 2 are significantly bigger ($p < 0.0001$) than the other loaded ones, since this peptide has a C10 lipid attached and making the peptide bigger and bulkier than the others. The encapsulation efficiency of Syn 2 micelles is 67% ± 9 which can also be explained by the differences between the sizes of the peptides and subsequently different folding.

The ZP of the empty micelles is -50.7 ± 2.3 mV, a significantly more negative value when compared to the loaded micelles ($p < 0.05$). The ZP of the loaded micelles is -47.0 ± 2.0 mV, -46.0 ± 2.4 mV and -47.3 ± 1.9 mV for L-Pmax, D-Pmax and Syn 2 respectively. The positive charge of the peptides is approximately +35 mV (**Figure 10 B**), which explains the reduction of ZP observed in the loaded micelles, either because the peptides are at the micelles' surface or free in solution. The high absolute value of ZP of the loaded micelles indicates very good stability in aqueous solution, due to the electrostatic repulsion preventing aggregation (184). The ZP value is expected to decrease in salt solutions due to the ionic shielding, but still maintaining a good stability (137).

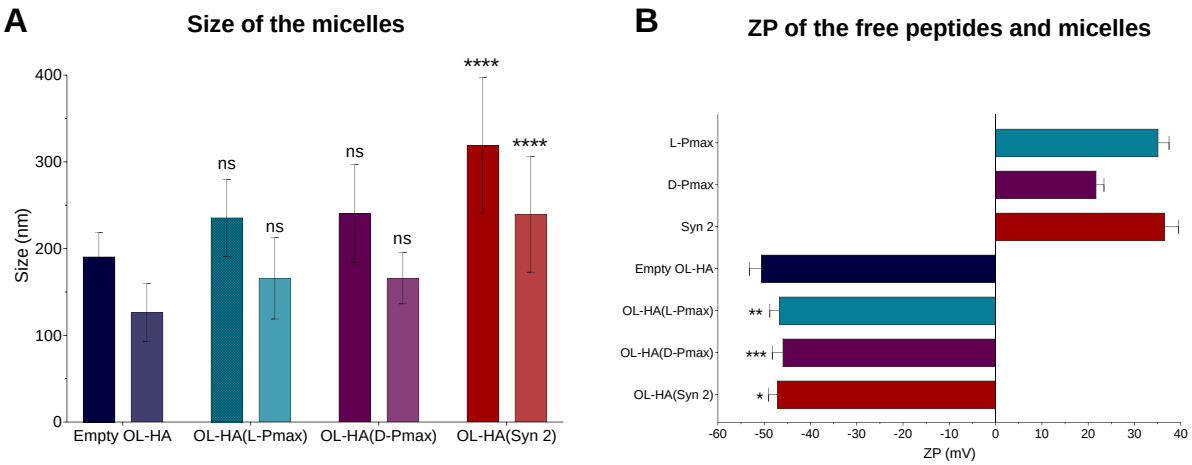

Figure 10 – Micelles size (nm) and zeta potential (mV) measured by DLS. (**A**) Size is illustrated in form of bars: Z-average (darker colour) and the size by number distribution (lighter colour), N=8-10. (**B**) ZP of the free peptides, empty OL-HA and the peptide-loaded micelles, N=7-9. Considering the empty OL-HA as control: ns, not significant, *$p < 0.05$, **$p < 0.01$, ***$p < 0.001$ and ****$p < 0.0001$.

Representative TEM micrographs of OL-HA and the D-Pmax loaded micelles are presented in **Figure 11 A** and **B**, respectively. TEM micrographs clearly show spherical micelles, with different sizes that explains the obtained PDI in DLS measurements of approximately 0.2. As expected, the hydrodynamic size measured

with DLS was larger than that observed by TEM, likely due to the dehydration of the particles. The size of the micelles was measured using Image J software (161), with empty OL-HA micelles presenting a diameter of 63 ± 38 nm and the D-Pmax-loaded OL-HA micelles showing a diameter of 54 ± 29 nm. Despite the good stability and electrostatic repulsion expected from the ZP results, the TEM images revealed a slight aggregation on the D-Pmax-loaded OL-HA micelles. These findings could explain the size differences between DLS and TEM measurements since the aggregates could be dispersing the light as big individual particles. However, it is also possible that the particle aggregation occurs as a result of freeze-drying of the particles, as this preservation process has previously shown to influence the stability of peptide and protein formulations, especially when no cryoprotectants are used (185,186).

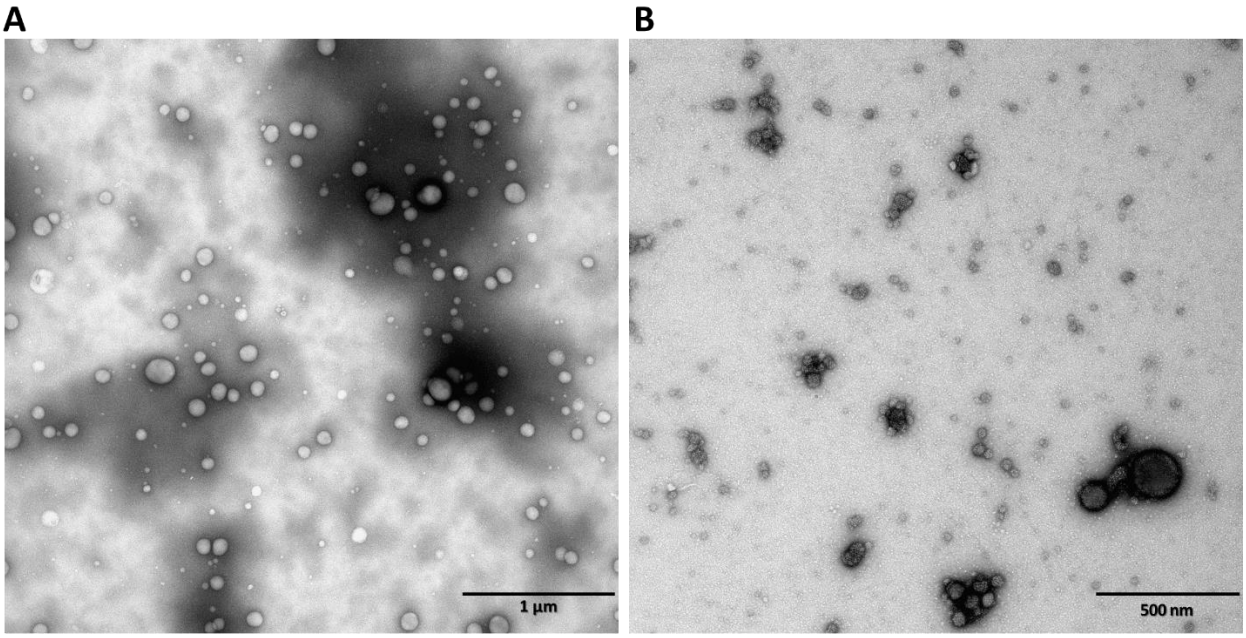

Figure 11 – TEM micrographs: (**A**) empty OL-HA micelles and (**B**) D-Pmax loaded micelles with a scale bar of 1 µm and 500 nm, respectively.

The release profile of all three different formulations was assessed over 96 h in HEPES a biorelevant medium, pH 7.4 using a dialysis membrane. The experiment was performed using exactly the same conditions for the free peptides as the control, to evaluate whether the dialysis membrane alone influences the movement of the peptides. These results are presented in **Figure 12 A** and **B**, except for Syn 2 that was not released from the dialysis membrane, probably due to its higher hydrophobicity and subsequently higher adsorption to the dialysis membrane. The release results of the peptide alone showed that after 8 h only 55% of the total amount of peptide could be quantified in the release medium. This amount was lower at later

time points, possibly due to peptide degradation (**Figure 12 A**). After 48 h the peak at the retention time corresponding to the peptide on the HPLC chromatogram was almost absent. Additionally, at this time point, there was an increase of other peaks, when compared to the calibration curve (free peptide in HEPES buffer) and to the 8 h time point (**Figure 19**, section "**Appendix**"). The increase in these peaks could be the result of peptide degradation, appearing fragments at smaller retention times. The D-form of this peptide showed to be more stable than the L- form during at least 72 h. The results also showed that after 6 h, the control D-Pmax reaches about 68 % of release from the dialysis membranes. Analysing these results, it seems that the membrane itself can influence the experiment, likely due to adsorption of the peptides to the device walls. This could explain why 100% release of the peptides was not observed.

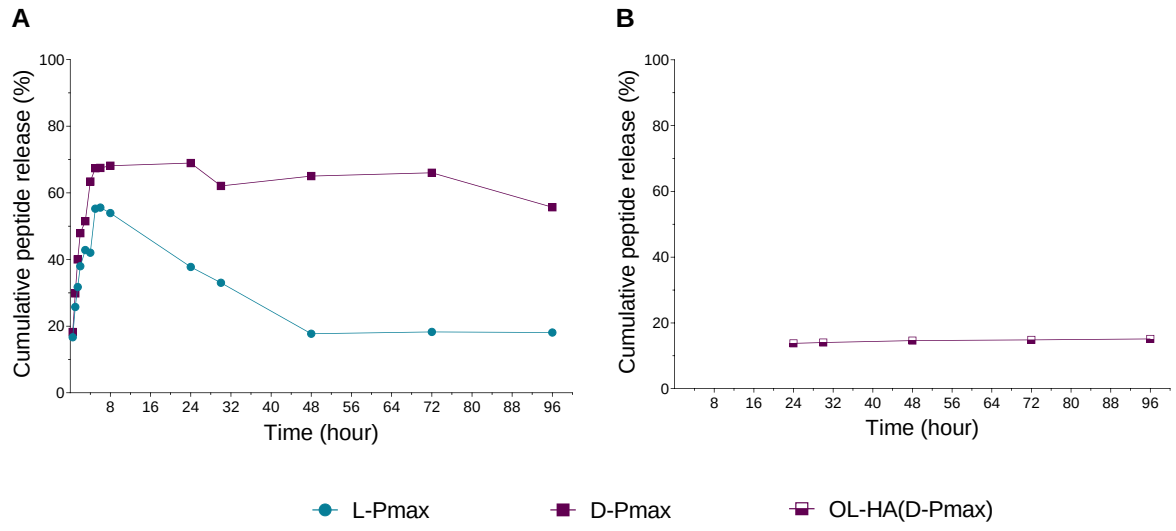

Figure 12 – Cumulative peptide release (%): (**A**) experimental control release of free L-Pmax and D-Pmax in HEPES pH 7.4 at 37°C (**B**) release of D-Pmax from OL-HA micelles, in HEPES pH 7.4 at 37°C. N=1

The L-Pmax released from the micelles was not possible to calculate, since the peaks observed on the HPLC chromatograms were not at the same retention time as in the calibration curve (4.7 min) (**Figure 20**, section "**Appendix**"). Additionally, 8 h after release there were no peaks on the HPLC chromatograms. These findings can be explained most likely due to *i)* a very strong binding of the peptide to the particles, *ii)* peptide degradation during the release or even a combination of both. Although, the lack of sensitivity of this method can also hamper the quantification of the released peptide.

In D-Pmax case, the release from the micelles appears to start only 24 h after, reaching 15 % (**Figure 12 B**), in addition to other peaks that could be due to either polymer or peptide degradation products.

Šmejkalová et al. also reported a slow release from this kind of micelles, only 12% of the loaded paclitaxel was released over 96 h of incubation (137). Despite the slow release, the cytotoxicity and antimicrobial activity was evaluated to gain a better understanding of the system.

4.2.2. Cytotoxicity of the peptides and the respective formulations

Effects on the viability of eukaryotes by the three Pmax peptides and the respective loaded micelles were assessed in hepatocytes (HepG2), endothelial cells (HUVEC), intestinal cells (Caco-2) and RBC. By evaluating the cytotoxicity of the formulations towards a range of cells, it will be possible to obtain a better understanding of the safety of the formulation when administered intravenously.

The results indicate that all three free peptides, both L-, D- form and the lipidated Pmax are not cytotoxic towards hepatocytes cell line (HepG2) up to 300 μg/mL, with viability higher than 90%. The viability at 600 μg/mL peptide concentration declines to approximately 40% viability (**Figure 13 A**). The four-parameter dose-response curve, a nonlinear regression model, was used to fit the data obtained for the cytotoxicity of the loaded micelles and determinate the IC_{50} of the peptides after 24 h. The results obtained equal to 361.5 μg/mL, 147 μg/mL and 285 μg/mL for L-Pmax, D-Pmax and Syn 2 respectively (**Figure 13 C**).

The results show that the encapsulation of all three peptides can increase the cell viability higher than 80% for at least 24 h incubation, as presented in **Figure 13**, **B** and **D**. Empty OL-HA micelles were also tested indicating no cytotoxicity (cell viability >80%) in the range 3.9 μg/mL to 1000 μg/mL (**Figure 21 A**, section "**Appendix**"). However, as this experiment was only performed once, this should be repeated having more replicas and at higher peptide concentrations to allow a better understanding of the peptide and micelles cytotoxicity profile.

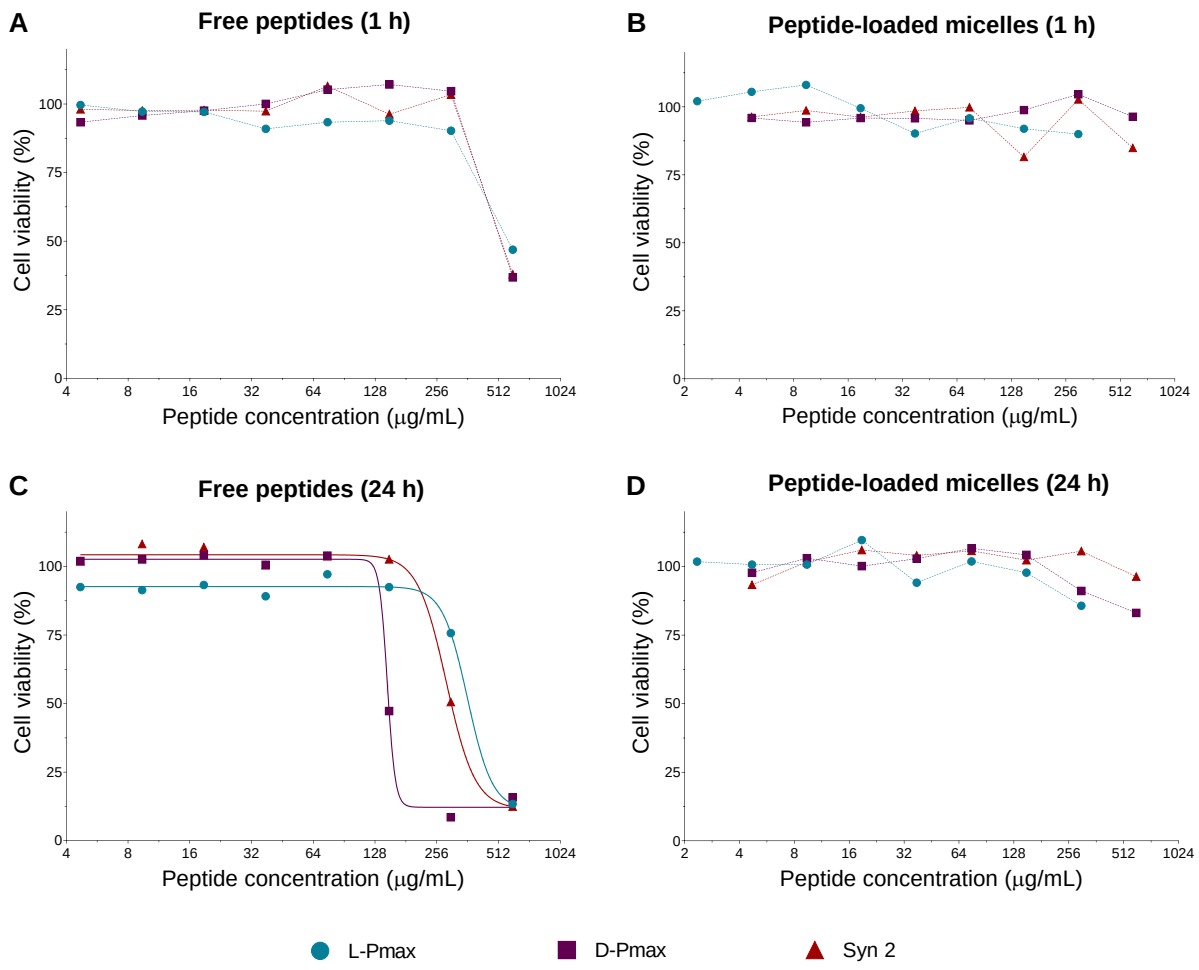

Figure 13 – Cytotoxicity towards HepG2 cell line of non-loaded peptides (**A** and **C**) and peptide-loaded micelles (**B** and **D**), after 1 h (**A** and **B**) or 24 h incubation (**C** and **D**); using MTS assay and represented as % cell viability related to the untreated control (cells with no peptide/micelles treatment). N=1

The endothelial cell line (HUVEC) appear to be more susceptible to both peptides and respective loaded micelles compared to the hepatic cells. The large variability in cell viability of this cell line, without an observed substantial drop in viability that could be clearly attributed to the formulations, suggests that the cells were not sufficiently confluent or attached to the wells to withstand the assay. Syn 2 have a higher cytotoxic effect with a larger decrease in cell viability (approximately 70%) compared to both L- and D- forms of Pmax. Both L- and the D- forms have the same tendency up to 300 μg/mL, but at 600 μg/mL the D- form show a higher cytotoxic effect (**Figure 14 A** and **C**). The higher toxicity correlates with the higher stability of the D-form showed above, which maintains the peptide active to exert both activity and toxicity. The empty micelles are moderately cytotoxic for concentration higher than 300 μg/mL (**Figure 21 B**, section "**Appendix**"),

explaining why every formulation seems to be slightly more cytotoxic than the free peptide at the same concentrations (**Figure 14 B** and **D**). To obtain more reliable results, this experiment should be repeated with additional passages of HUVEC cells and in more biological and technical replicates.

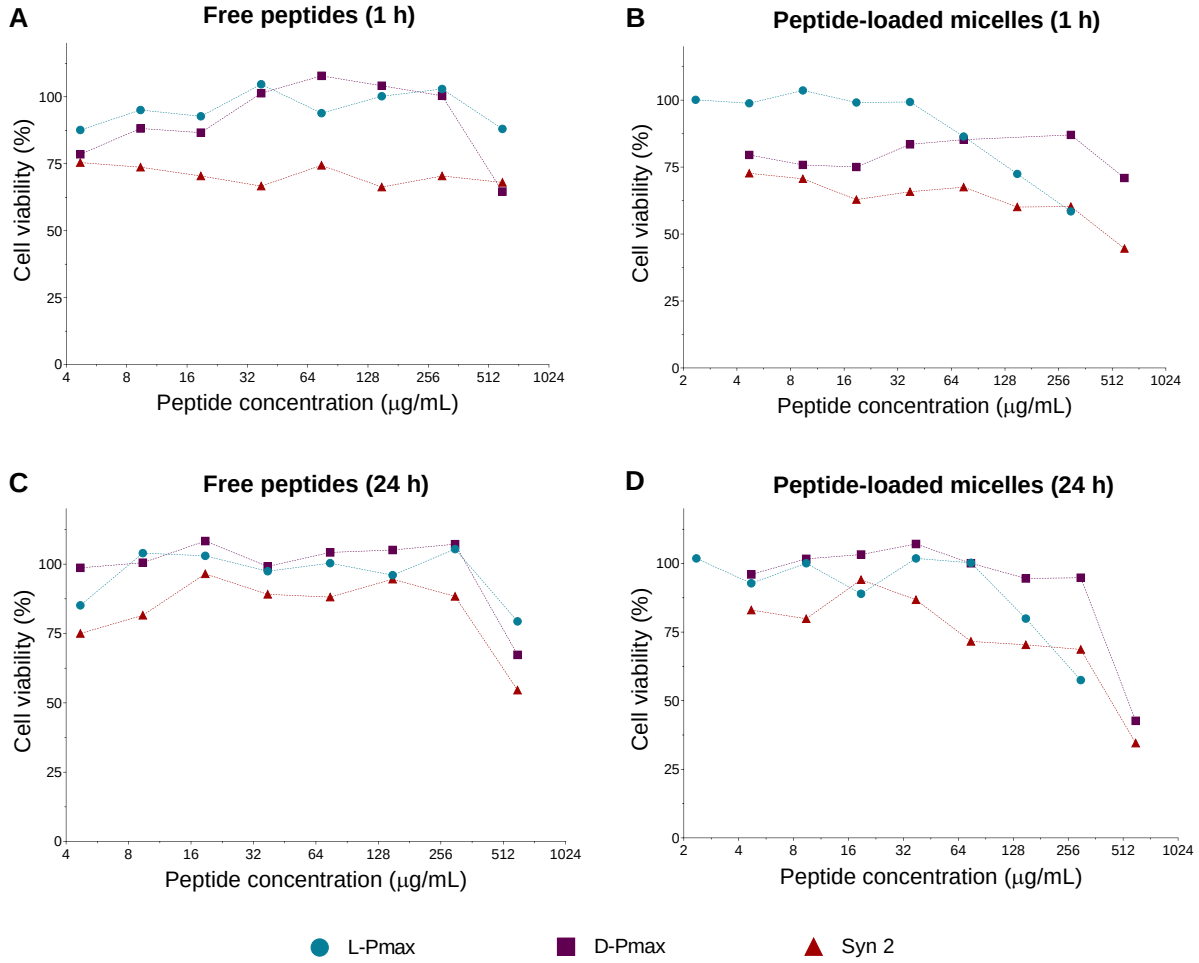

Figure 14 – Cytotoxicity towards HUVEC cell line of non-loaded peptides (**A** and **C**) and peptide-loaded micelles (**B** and **D**), after 1 h (**A** and **B**) and after 24 h (**C** and **D**); using MTS assay and represented as % cell viability related to the untreated control. N=1

The cytotoxicity of all three peptides and formulations was also assessed towards the intestinal cell line (Caco-2) in a peptide concentration range of 10 μg/mL to 300 μg/mL. As expected, the peptide with lower cytotoxicity is L-Pmax, followed by its D-form and Syn 2 the peptide with higher hydrophobicity (**Figure 15 A**). A nonlinear regression model (four-parameter dose-response curve), was again applied to fit the results and determinate the IC_{50} of the peptides (N=6). L-Pmax IC_{50} equals to 175 μg/mL, D-Pmax IC_{50} is 91.6 μg/mL and for Syn 2, 82.4 μg/mL. All different formulations were also tested in the same conditions and

with the same peptide concentrations. The percentage of intestinal cell viability was higher than 90% up to 300 μg/mL peptide concentration (**Figure 15 B**), eliminating completely any signs of peptide cytotoxicity.

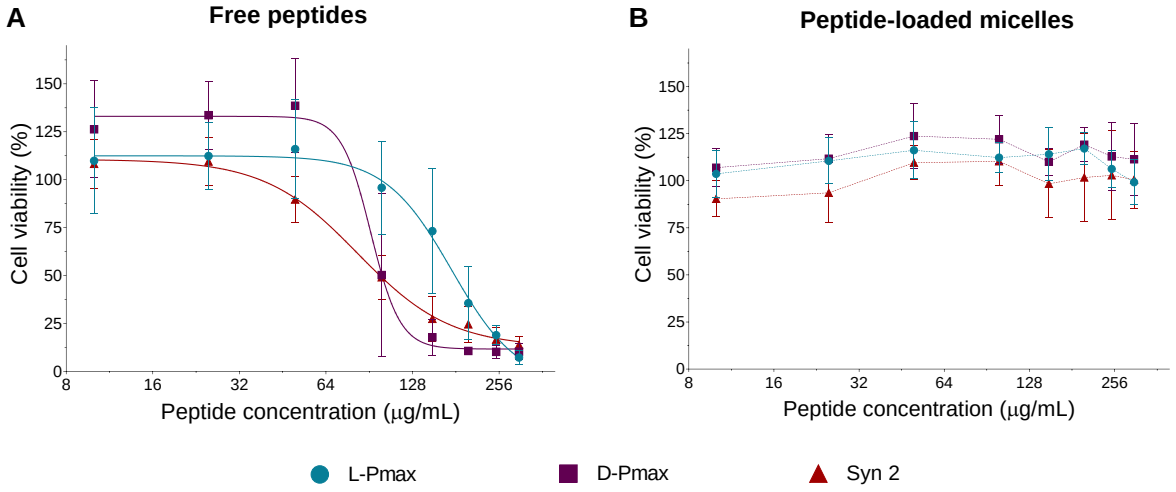

Figure 15 – Cytotoxicity towards Caco-2 cell line of (**A**) non-loaded peptides and (**B**) peptide-loaded micelles; using MTS assay and represented as % cell viability related to the untreated control. Mean ± SD; N=6

In general, encapsulating the peptides also reduces the hemolytic effect almost completely in the tested range from 5 μg/mL to 300 μg/mL peptide concentration. Hemolysis data is most frequently presented as IC_{10} and IC_{50}, indicating the concentration of drug that results in lysis of 10 and 50% of RBC, respectively. Both L- and D- form of Pmax presented a hemolytic effect lower than approximately 20% in the tested concentration range. Despite an already low hemolytic effect of the peptides, their hemolytic effect was further reduced after incorporation into the OL-HA micelles (**Figure 16 A** and **B**). For the peptide L-Pmax, an IC_{10} of 5 μg/mL was observed, but after encapsulation in OL-HA particles the IC_{10} increased to approximately 200 μg/mL, indicating a 40-fold reduction in RBC toxicity. For D-Pmax, the IC_{10} was also 5 μg/mL and similarly increased to approximately 200 μg/mL after encapsulation, indicating substantially improved safety of the peptides. According to the nonlinear regression fit, the four-parameter dose-response curve, a Syn 2 concentration of 144.2 μg/mL is enough to lyse 50% of the erythrocytes (**Figure 16 C**). Syn 2 is more hemolytic than the other peptides, which is consistent with previous reports, that showed higher cytotoxicity levels to greater hydrophobic peptides (187). Despite that, as for L- and D-Pmax peptides, Syn 2 cytotoxicity

was reduced to half after encapsulation into OL-HA micelles. Both empty micelles and the polymer suspension appear not to have substantial hemolytic effects (**Figure 16 D**).

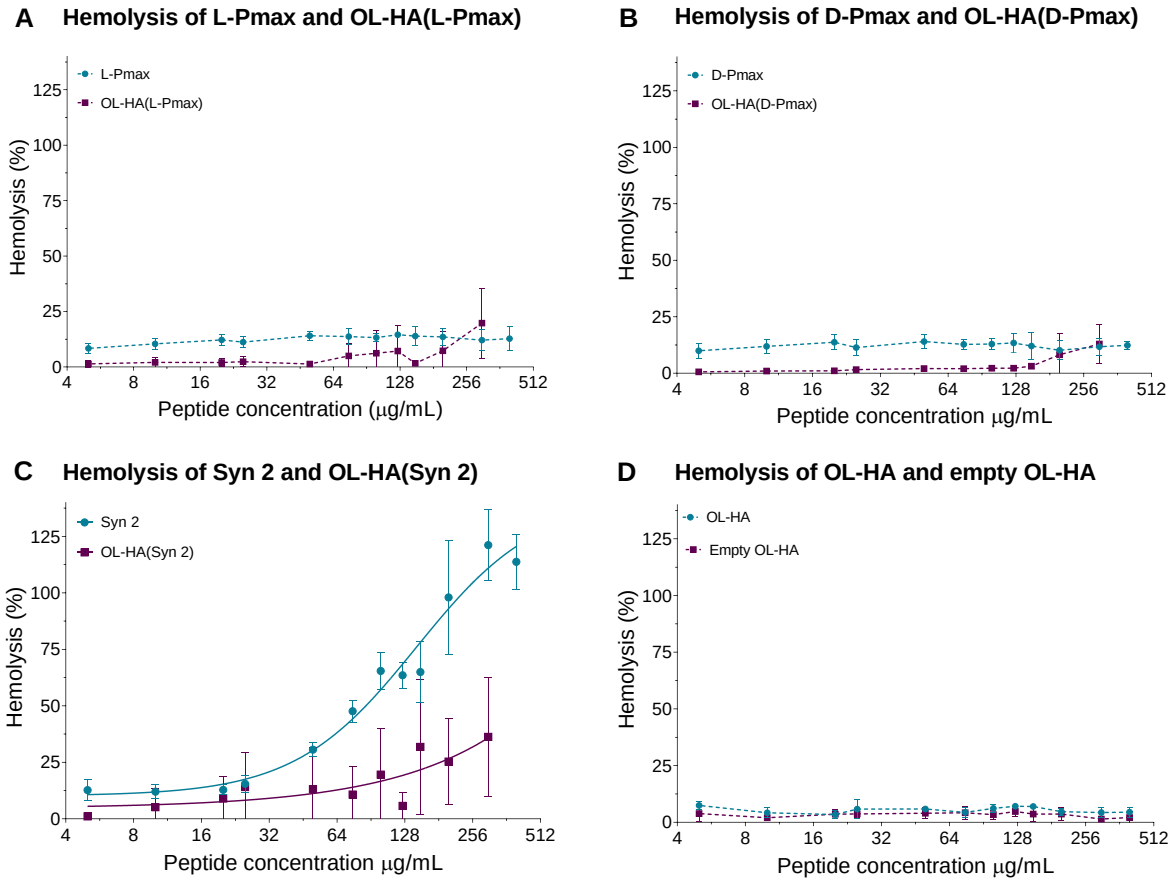

Figure 16 – Hemolytic effect of non-loaded peptides and respective loaded micelles (**A**) L-Pmax (**B**) D-Pmax (**C**) Syn 2 and (**D**) polymeric suspension (OL-HA) and empty OL-HA micelles; % hemolysis related to the control treated with 0.2% SDS; Mean ± SD; N=3-9

In summary, the encapsulation of the peptides into micelles can improve their therapeutic effect. The results indicate that these formulations can be used to deliver the peptides by intravenous administration at a wide range of concentrations.

4.2.3. Antibacterial activity

Bacterial growth inhibition is most frequently evaluated in form of MIC, which is the lowest peptide concentration that inhibits bacterial growth. When the three bacteria strains were exposed to the peptides and peptide-loaded micelles, the MIC generally remained the same, indicating that, although the peptide was encapsulated, it exerted the same effect as a free peptide solution (**Table 3**). Here we tested a range of concentrations that were sub-cytotoxic (≤ 128 µg/mL). In some cases, a two-fold increase in MIC is observed, however, the precision of the broth dilution method is considered to be plus or minus 1 two-fold concentration (188). *S. aureus* showed to be largely resistant to L-Pmax and Syn 2 and their corresponding formulations. Studies reported that membrane-active cationic antibacterial peptides on their way to the cytoplasmic membrane are exposed to different molecules, exhibiting different affinities which may reduce their antimicrobial effect. (189). The interaction of the tested cationic peptides with the anionic lipoteichoic acids, present on Gram-positive bacterial cell wall, may reduce the local concentration on the cytoplasmic membrane (189), which cloud explain the lower activity against *S. aureus*. The lowest MIC values were observed for D-Pmax and OL-HA(D-Pmax) particles towards all three pathogens, indicating the highest antimicrobial activity of this peptide and this formulation. Manabe and Kawasaki also reported higher antimicrobial activity of the antimicrobial peptide D-form KLKLLLLLKLK-NH2 than the L-form via a specific association with bacterial cell wall components, including peptidoglycan (190).

Table 3 – MIC (µg/mL) of the three peptides and respective peptide-loaded micelles. N=6

Sample	MIC (µg/mL)		
	***S. aureus* 15981**	***E. coli* ATCC 25922**	***P. aeruginosa* PA01**
L-Pmax	>128	32	16
OL-HA(L-Pmax)	>128	64	32
D-Pmax	8	16	4
OL-HA(D-Pmax)	16	16	8
Syn 2	>128	128	32
OL-HA(Syn 2)	>128	128	64

To our knowledge, the antimicrobial activity of these peptides has never been reported before. Comparing these finding with the literature available on the antibacterial effect of Pen towards *E. coli* (85), it seems that both L-and D-Pmax has lower MIC values, even when encapsulated. When comparing the antibacterial activity of these peptides against *P. aeruginosa* and *S. aureus* it is important to keep in mind that the antibacterial assays may have been performed on different bacterial strains (**Table 1**, section "***Introduction***"). Despite that, these three peptides, encapsulated or not, present higher antibacterial potential than Pen against some of the strains reported.

To assess whether bacterial biofilm growth can be inhibited at concentrations below MIC, a biofilm inhibition assay on *P. aeruginosa* was performed. This bacterium was chosen as it is a better biofilm forming pathogen than *S. aureus* or *E. coli* (191,192). Overall, the results were in agreement with the MIC results, with biofilm formation occurring below MIC concentrations and sometimes also at MIC (**Figure 17 A**, **B** and **C**). In general, D-Pmax and OL-HA(D-Pmax) resulted in less biofilm formation at sub-MIC concentrations in comparison to L-Pmax and Syn 2 and their respective peptide-loaded micelles. An overproduction of biofilm in response to low antimicrobial concentrations is a natural defence system of bacteria (193) and may indicate that faster resistance will develop towards those antimicrobials. As a result, D-Pmax and OL-HA(D-Pmax) particles are most favourable for antimicrobial therapies due to low biofilm overproduction at sub-MIC concentrations.

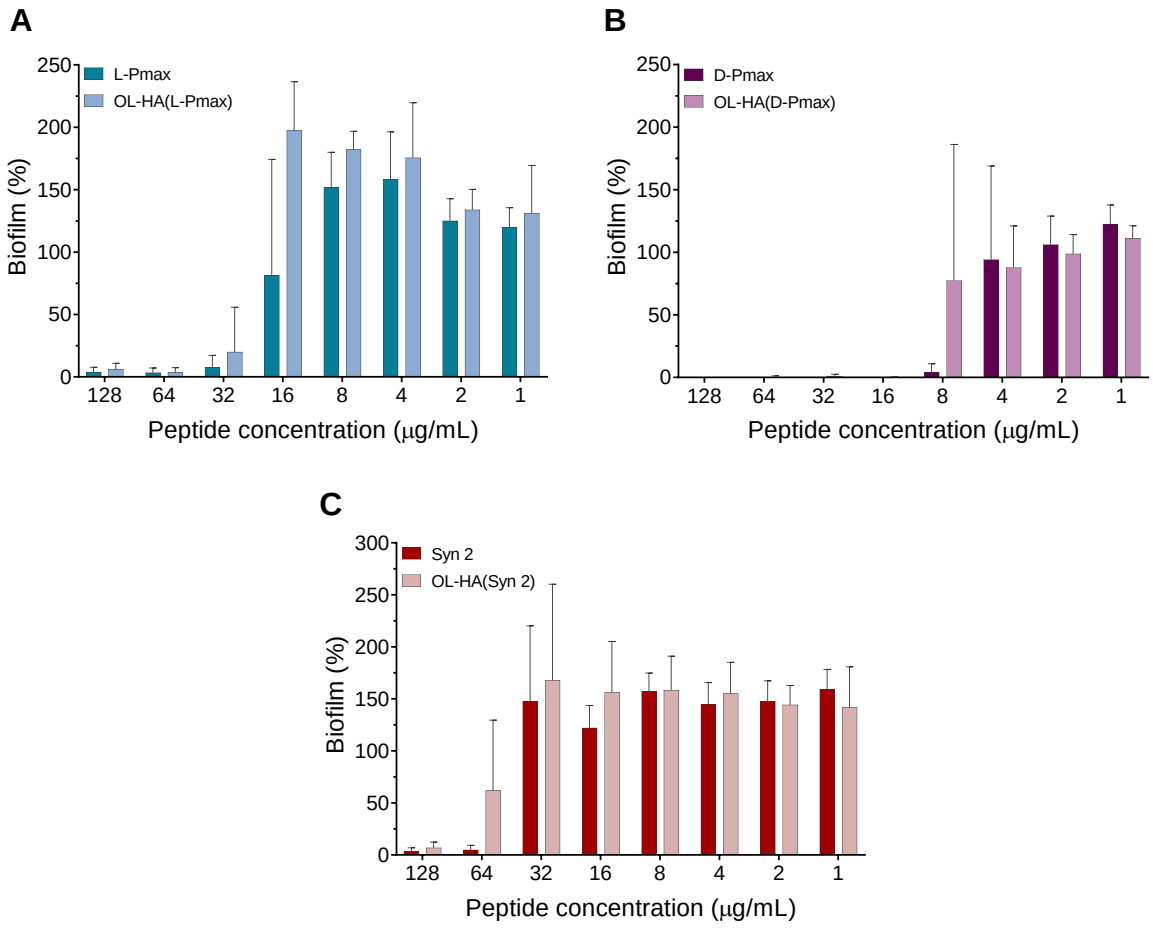

Figure 17 – Inhibition of P. aeruginosa biofilm formation after 20 h incubation with the peptides and peptide-loaded micelles; % biofilm related to the untreated control (100% biofilm). Mean ± SD; N=6.

Despite the slow release from the delivery system, these micelles can be an excellent option to tackle bacterial infections, especially when using D-Pmax as the peptide. The D-Pmax peptides showed the highest stability, medium cytotoxicity, best antimicrobial activity and low biofilm formation at sub-inhibitory concentrations. After encapsulation, despite the limited release of the peptide from the particles, the antimicrobial activity of the peptide was maintained and simultaneously the cytotoxicity of the peptide was reduced. Altogether, these findings indicate that OL-HA micelles are a very good delivery system for improving the properties of peptides with antimicrobial properties.

5. Conclusion

The continuously need for highly efficient therapeutic antibacterial formulations motivated this research aiming to develop and characterize novel micelles to encapsulate and deliver antimicrobial peptides. In this work, a preparation method for peptide-loaded OL-HA micelles was established and optimized. The OL-HA polymer was used to produce spherical anionic and hydrophilic polymeric micelles, with a hydrodynamic diameter range of 100 – 300 nm depending on the peptide encapsulated. The high encapsulation efficiency of these micelles indicates that they are well suited as a delivery system for these peptides. In order to obtain best antimicrobial activity, the goal is usually for an antimicrobial formulation to have a burst release of the therapeutic agent, to eradicate the pathogen as quickly as possible, which decreases the possibility for bacteria develop antibiotic resistance (194). However, these micelles, which show a very slow release over time, have shown to maintain the antimicrobial activity of the encapsulated peptides. These findings may indicate a synergistic effect between the polymeric carrier and the peptide.

The cytotoxicity assessment of both non-loaded peptides and respective formulation showed that, in general, the encapsulation of the peptides can substantially reduce their cytotoxicity towards hepatic, endothelial, intestinal and RBC. All three CPPs, both L- and D-Pmax, and Syn 2, have antibacterial activity against *S. aureus*, *E. coli* and *P. aeruginosa*, in some strains even higher activity than their precursor Pen (85,87,88). The encapsulation of these peptides did not influence the MIC values, not more than one two-fold dilution. The evaluation of the effect of these micelles on biofilm formation indicated that they can prevent the growth of biofilm at concentrations higher than the MIC values.

In conclusion, these formulations reveal to have the potential to tackle bacterial infections while reducing side effects associated with the peptides. The D-Pmax loaded micelles are the most promising of all three, with small particles sizes, high peptide encapsulation and lower peptide degradation rates. Encapsulation in OL-HA particles reduced the peptide cytotoxicity without compromising its antibacterial and antibiofilm activity.

6. Future perspectives

In order to further improve the formulation, additional optimization of the micelle preparation method should be performed, ideally in triplicate to obtain the most reliable results. Other parameters or methodologies such as different sonication amplitudes and duration, different flow rates using microfluidics assay and also test its peptide adsorption could be included in the evaluation, which was not possible to assess during this research project due to time constraints and the Covid-19 pandemic.

The therapeutic potential of these formulations could be further improved by boosting their release profile to a faster release incorporating a trigger system, for example, temperature, pH or enzymes (194–196). This could be done by forming the particles using a different polymer, such as chitosan or using the same polymer but with different chemical crosslinks. Additionally, as the release for the delivery system is thought to be triggered by the presence of salts, the formation of the particles in presence of salts could result in looser binding of the peptide to the polymer, also allowing for faster release. Finally, the peptide-loaded delivery system could be evaluated for other purposes or administration routes, as the slow release can also be beneficial in some antimicrobial therapies, to ensure a proper antibiotic concentration for extended periods, for example in tissue engineering and regenerative medicine (194).

7. References

1. World Health Organization. Antimicrobial resistance. 2018. Available from: https://www.who.int/news-room/fact-sheets/detail/antimicrobial-resistance#
2. Cassini A, Högberg LD, Plachouras D, Quattrocchi A, Hoxha A, Simonsen GS, et al. Attributable deaths and disability-adjusted life-years caused by infections with antibiotic-resistant bacteria in the EU and the European Economic Area in 2015: a population-level modelling analysis. Lancet Infect Dis. 2019 Jan;19(1):56–66.
3. O'Neill J. Review on Antimicrobial Resistance. Antimicrobial Resistance: Tackling a crisis for the health and wealth of nations. Review on Antimicrobial Resistance, London, United Kingdom. 2014.
4. Brooks BD, Brooks AE. Therapeutic strategies to combat antibiotic resistance. Adv Drug Deliv Rev. 2014;78:14–27.
5. Prestinaci F, Pezzotti P, Pantosti A. Antimicrobial resistance: A global multifaceted phenomenon. Pathog Glob Health. 2015;109(7):309–18.
6. Li B, Webster TJ. Bacteria antibiotic resistance: New challenges and opportunities for implant-associated orthopedic infections. J Orthop Res. 2018 Aug 11;36(1):22–32.
7. Pendleton JN, Gorman SP, Gilmore BF. Clinical relevance of the ESKAPE pathogens. Expert Rev Anti Infect Ther. 2013;11(3):297–308.
8. Rice LB. Federal Funding for the Study of Antimicrobial Resistance in Nosocomial Pathogens: No ESKAPE. J Infect Dis. 2008 Apr 15;197(8):1079–81.
9. Pogue JM, Kaye KS, Cohen DA, Marchaim D. Appropriate antimicrobial therapy in the era of multidrug-resistant human pathogens. Clin Microbiol Infect. 2015 Apr 1;21(4):302–12.
10. Santajit S, Indrawattana N. Mechanisms of Antimicrobial Resistance in ESKAPE Pathogens. Biomed Res Int. 2016;2016.
11. World Health Organization. 2019 antibacterial agents in clinical development: an analysis of the antibacterial clinical development pipeline. Geneva; 2019.
12. Plackett B. Why big pharma has abandoned antibiotics. Vol. 586, Nature. England; 2020. p. S50–2.
13. Sørum H, L'Abée-Lund TM. Antibiotic resistance in food-related bacteria - A result of

interfering with the global web of bacterial genetics. Int J Food Microbiol. 2002;78(1–2):43–56.

14. Mulani MS, Kamble EE, Kumkar SN, Tawre MS, Pardesi KR. Emerging strategies to combat ESKAPE pathogens in the era of antimicrobial resistance: A review. Front Microbiol. 2019;10.
15. Mandal SM, Roy A, Ghosh AK, Hazra TK, Basak A, Franco OL. Challenges and future prospects of antibiotic therapy: From peptides to phages utilization. Vol. 5, Frontiers in Pharmacology. Frontiers Research Foundation; 2014.
16. Kaur I. Novel Strategies to Combat Antimicrobial Resistance. J Infect Dis Ther. 2016;4(4).
17. Lagadinou M, Onisor MO, Rigas A, Musetescu D-V, Gkentzi D, Assimakopoulos SF, et al. Antimicrobial Properties on Non-Antibiotic Drugs in the Era of Increased Bacterial Resistance. Antibiotics. 2020;9(3):107.
18. Secor PR, Sweere JM, Michaels LA, Malkovskiy A V., Lazzareschi D, Katznelson E, et al. Filamentous bacteriophage promote biofilm assembly and function. Cell Host Microbe. 2015 Nov 11;18(5):549–59.
19. Teixeira MC, Carbone C, Sousa MC, Espina M, Garcia ML, Sanchez-Lopez E, et al. Nanomedicines for the Delivery of Antimicrobial Peptides (AMPs). Nanomaterials. 2020;10(3):560.
20. Cavalieri F, Tortora M, Stringaro A, Colone M, Baldassarri L. Nanomedicines for antimicrobial interventions. Vol. 88, Journal of Hospital Infection. W.B. Saunders Ltd; 2014. p. 183–90.
21. Wagner V, Hüsing B, Gaisser S, Bock A-K. Nanomedicine: Drivers for development and possible impacts. 23494 EN. JRC-IPTS, EUR. 2008.
22. Salomoni R, Léo P, Montemor AF, Rinaldi BG, Rodrigues MFA. Antibacterial effect of silver nanoparticles in Pseudomonas aeruginosa. Nanotechnol Sci Appl. 2017 Jun 29;10:115–21.
23. Wang L, Hu C, Shao L. The antimicrobial activity of nanoparticles: Present situation and prospects for the future. Int J Nanomedicine. 2017 Feb 14;12:1227–49.
24. Fernando S, Gunasekara T, Holton J. Antimicrobial Nanoparticles: applications and mechanisms of action. Sri Lankan J Infect Dis. 2018 May 6;8(1):2.

25. Ponnappan N, Budagavi DP, Yadav BK, Chugh A. Membrane-Active Peptides from Marine Organisms—Antimicrobials, Cell-Penetrating Peptides and Peptide Toxins: Applications and Prospects. Probiotics Antimicrob Proteins. 2015;7(1):75–89.
26. Langel Ü. Classes and Applications of Cell-Penetrating Peptides. In: CPP, Cell-Penetrating Peptides. Singapore: Springer Nature Pte Ltd.; 2019. p. 29–82.
27. Langel Ü. Introduction. In: CPP, Cell-Penetrating Peptides. Singapore: Springer Nature Pte Ltd.; 2019. p. 1–28.
28. Rydberg HA, Carlsson N, Nordén B. Membrane interaction and secondary structure of de novo designed arginine-and tryptophan peptides with dual function. Biochem Biophys Res Commun. 2012;427(2):261–5.
29. Wang Q, Hong G, Johnson GR, Pachter R, Cheung MS. Biophysical properties of membrane-active peptides based on micelle modeling: A case study of cell-penetrating and antimicrobial peptides. J Phys Chem B. 2010;114(43):13726–35.
30. Nekhotiaeva N, Elmquist A, Rajarao GK, Hällbrink M, Langel Ü, Good L. Cell entry and antimicrobial properties of eukaryotic cell-penetrating peptides. FASEB J. 2004 Dec 4;18(2):394–6.
31. Ciobanasu C, Kubitscheck U. Cell-Penetrating Peptides Targeting and Distorting Biological Membranes. In: Wandelt K, editor. Surface and Interface Science: Liquid and Biological Interfaces. First Edit. Wiley-VCH Verlag GmbH & Co. KGaA; 2020. p. 441–69.
32. Splith K, Neundorf I. Antimicrobial peptides with cell-penetrating peptide properties and vice versa. Eur Biophys J. 2011;40:387–97.
33. Henriques ST, Melo MN, Castanho MARB. Cell-penetrating peptides and antimicrobial peptides: How different are they? Biochem J. 2006;399(1):1–7.
34. Kang HK, Kim C, Seo CH, Park Y. The therapeutic applications of antimicrobial peptides (AMPs): a patent review. J Microbiol. 2017;55(1):1–12.
35. Reddy KVR, Yedery RD, Aranha C. Antimicrobial peptides: Premises and promises. Int J Antimicrob Agents. 2004 Dec 1;24(6):536–47.
36. Malmsten M. Antimicrobial peptides. Ups J Med Sci. 2014;119(2):199–204.
37. Nakatsuji T, Gallo RL. Antimicrobial Peptides: Old Molecules with New Ideas. J Invest

Dermatol. 2012 Mar 1;132(3 Part 2):887–95.

38. Pirtskhalava M, Gabrielian A, Cruz P, Griggs HL, Squires RB, Hurt DE, et al. DBAASP v.2: an enhanced database of structure and antimicrobial/cytotoxic activity of natural and synthetic peptides. Nucleic Acids Res. 2015th ed. 2015 Jan 4;44(D1):D1104–12.
39. Felício MR, Silva ON, Gonçalves S, Santos NC, Franco OL. Peptides with dual antimicrobial and anticancer activities. Front Chem. 2017;5(5).
40. Martin-Serrano Á, Gómez R, Ortega P, Mata FJD La, de la Mata FJ. Nanosystems as vehicles for the delivery of antimicrobial peptides (Amps). Pharmaceutics. 2019;11(9):1–24.
41. Wang G. Database-guided discovery of potent peptides to combat HIV-1 or superbugs. Pharmaceuticals. 2013;6(6):728–58.
42. Pasupuleti M, Schmidtchen A, Malmsten M. Antimicrobial peptides: Key components of the innate immune system. Crit Rev Biotechnol. 2012;32(2):143–71.
43. Hilchie AL, Wuerth K, Hancock REW. Immune modulation by multifaceted cationic host defense (antimicrobial) peptides. Nat Chem Biol. 2013;9(12):761–8.
44. Lai Y, Gallo RL. AMPed up immunity: how antimicrobial peptides have multiple roles in immune defense. Trends Immunol. 2009;30(3):131–41.
45. Hancock REW, Nijnik A, Philpott DJ. Modulating immunity as a therapy for bacterial infections. Nat Rev Microbiol. 2012;10(4):243–54.
46. Zhang SK, Song JW, Gong F, Li SB, Chang HY, Xie HM, et al. Design of an α-helical antimicrobial peptide with improved cell-selective and potent anti-biofilm activity. Sci Rep. 2016;6(1):1–13.
47. Gwyer Findlay E, Currie SM, Davidson DJ. Cationic host defence peptides: Potential as antiviral therapeutics. BioDrugs. 2013;27(5):479–93.
48. Kumar P, Kizhakkedathu JN, Straus SK. Antimicrobial peptides: Diversity, mechanism of action and strategies to improve the activity and biocompatibility in vivo. Biomolecules. 2018;8(1):4.
49. Pfalzgraff A, Brandenburg K, Weindl G. Antimicrobial peptides and their therapeutic potential for bacterial skin infections and wounds. Front Pharmacol. 2018;9:281.
50. Dathe M, Nikolenko H, Meyer J, Beyermann M, Bienert M. Optimization of the

antimicrobial activity of magainin peptides by modification of charge. FEBS Lett. 2001;501(2–3):146–50.

51. Yin LM, Edwards MA, Li J, Yip CM, Deber CM. Roles of hydrophobicity and charge distribution of cationic antimicrobial peptides in peptide-membrane interactions. J Biol Chem. 2012;287(10):7738–45.
52. Greber KE., Dawgul M. Antimicrobial Peptides Under Clinical Trials. Curr Top Med Chem. 2017;17(5):620–8.
53. Frankel AD, Pabo CO. Cellular uptake of the tat protein from human immunodeficiency virus. Cell. 1988;55(6):1189–93.
54. Joliot A, Pernelle C, Deagostini-Bazin H, Prochiantz A. Antennapedia homeobox peptide regulates neural morphogenesis. Proc Natl Acad Sci. 1991;88(5):1864–8.
55. Agrawal P, Bhalla S, Usmani SS, Singh S, Chaudhary K, Raghava GPS, et al. CPPsite 2.0: A repository of experimentally validated cell-penetrating peptides. Nucleic Acids Res. 2016;44(D1):D1098–103.
56. Koren E, Torchilin VP. Cell-penetrating peptides: Breaking through to the other side. Trends Mol Med. 2012;18(7):385–93.
57. Mäe M, Langel Ü. Cell-penetrating peptides as vectors for peptide, protein and oligonucleotide delivery. Curr Opin Pharmacol. 2006;6(5):509–14.
58. Fischer R, Fotin-Mleczek M, Hufnagel H, Brock R. Break on through to the other side - Biophysics and cell biology shed light on cell-penetrating peptides. ChemBioChem. 2005;6(12):2126–42.
59. Boisguerin P, Giorgi J-M, Barrere-Lemaire S. CPP-conjugated Anti-apoptotic Peptides as Therapeutic Tools of Ischemiareperfusion Injuries. Curr Pharm Des. 2013;19(16):2970–8.
60. Nasrollahi SA, Fouladdel S, Taghibiglou C, Azizi E, Farboud ES. A peptide carrier for the delivery of elastin into fibroblast cells. Int J Dermatol. 2012;51(8):923–9.
61. Lehto T, Kurrikoff K, Langel Ü. Cell-penetrating peptides for the delivery of nucleic acids. Expert Opin Drug Deliv. 2012;9(7):823–36.
62. Margus H, Padari K, Pooga M. Cell-penetrating peptides as versatile vehicles for oligonucleotide delivery. Mol Ther. 2012;20(3):525–33.

63. Chen B, Xu W, Pan R, Chen P. Design and characterization of a new peptide vector for short interfering RNA delivery. J Nanobiotechnology. 2015;13(1):39.
64. Shi NQ, Gao W, Xiang B, Qi XR. Enhancing cellular uptake of activable cell-penetrating peptide-doxorubicin conjugate by enzymatic cleavage. Int J Nanomedicine. 2012;7:1613–21.
65. Qian Z, LaRochelle JR, Jiang B, Lian W, Hard RL, Selner NG, et al. Early endosomal escape of a cyclic cell-penetrating peptide allows effective cytosolic cargo delivery. Biochemistry. 2014;53(24):4034–46.
66. Dekiwadia CD, Lawrie AC, Fecondo J V. Peptide-mediated cell penetration and targeted delivery of gold nanoparticles into lysosomes. J Pept Sci. 2012;18(8):527–34.
67. Xia H, Gao X, Gu G, Liu Z, Hu Q, Tu Y, et al. Penetratin-functionalized PEG-PLA nanoparticles for brain drug delivery. Int J Pharm. 2012;436(1–2):840–50.
68. Mei L, Fu L, Shi K, Zhang Q, Liu Y, Tang J, et al. Increased tumor targeted delivery using a multistage liposome system functionalized with RGD, TAT and cleavable PEG. Int J Pharm. 2014;468(1–2):26–38.
69. Gupta N, Ibrahim HM, Ahsan F. Peptide-micelle hybrids containing fasudil for targeted delivery to the pulmonary arteries and arterioles to treat pulmonary arterial hypertension. J Pharm Sci. 2014;103(11):3743–53.
70. Milletti F. Cell-penetrating peptides: Classes, origin, and current landscape. Drug Discov Today. 2012;17(15–16):850–60.
71. Guidotti G, Brambilla L, Rossi D. Cell-Penetrating Peptides: From Basic Research to Clinics. Trends Pharmacol Sci. 2017;38(4):406–24.
72. Marks JR, Placone J, Hristova K, Wimley WC. Spontaneous membrane-translocating peptides by orthogonal high-throughput screening. J Am Chem Soc. 2011;133(23):8995–9004.
73. Jobin ML, Blanchet M, Henry S, Chaignepain S, Manigand C, Castano S, et al. The role of tryptophans on the cellular uptake and membrane interaction of arginine-rich cell penetrating peptides. Biochim Biophys Acta - Biomembr. 2015;1848(2):593–602.
74. Kamide K, Nakakubo H, Uno S, Fukamizu A. Isolation of novel cell-penetrating peptides

from a random peptide library using in vitro virus and their modifications. Int J Mol Med. 2010;25(1):41–51.

75. Christiaens B, Symoens S, Vanderheyden S, Engelborghs Y, Joliot A, Prochiantz A, et al. Tryptophan fluorescence study of the interaction of penetratin peptides with model membranes. Eur J Biochem. 2002;269(12):2918–26.
76. Ziegler A. Thermodynamic studies and binding mechanisms of cell-penetrating peptides with lipids and glycosaminoglycans. Adv Drug Deliv Rev. 2008;60(4–5):580–97.
77. Khafagy ES, Kamei N, Nielsen EJB, Nishio R, Takeda-Morishita M. One-month subchronic toxicity study of cell-penetrating peptides for insulin nasal delivery in rats. Eur J Pharm Biopharm. 2013;85(3 Part A):736–43.
78. Polyansky AA, Volynsky PE, Arseniev AS, Efremov RG. Adaptation of a membrane-active peptide to heterogeneous environment. II. The role of mosaic nature of the membrane surface. J Phys Chem B. 2009;113(4):1120–6.
79. Almeida PF, Pokorny A. Mechanisms of antimicrobial, cytolytic, and cell-penetrating peptides: From kinetics to thermodynamics. Biochemistry. 2009;48(34):8083–93.
80. Adão R, Nazmi K, Bolscher J, Bastos M. C- and N-truncated antimicrobial peptides from LFampin 265 - 284: Biophysical versus microbiology results. J Pharm Bioallied Sci. 2011;3(1):60–9.
81. Sitaram N, Nagaraj R. Interaction of antimicrobial peptides with biological and model membranes: Structural and charge requirements for activity. Biochim Biophys Acta - Biomembr. 1999;1462(1–2):29–54.
82. Zhu WL, Shin SY. Effects of dimerization of the cell-penetrating peptide Tat analog on antimicrobial activity and mechanism of bactericidal action. J Pept Sci. 2009;15(5):345–52.
83. Zhu WL, Lan H, Park IS, Kim J Il, Jin HZ, Hahm KS, et al. Design and mechanism of action of a novel bacteria-selective antimicrobial peptide from the cell-penetrating peptide Pep-1. Biochem Biophys Res Commun. 2006;349(2):769–74.
84. Palm C, Netzereab S, Hällbrink M. Quantitatively determined uptake of cell-penetrating peptides in non-mammalian cells with an evaluation of degradation and antimicrobial effects. Peptides. 2006;27(7):1710–6.

85. Bahnsen JS, Franzyk H, Sandberg-Schaal A, Nielsen HM. Antimicrobial and cell-penetrating properties of penetratin analogs: Effect of sequence and secondary structure. Biochim Biophys Acta - Biomembr. 2013;1828(2):223–32.
86. Brand GD, Magalhães MTQ, Tinoco MLP, Aragão FJL, Nicoli J, Kelly SM, et al. Probing Protein Sequences as Sources for Encrypted Antimicrobial Peptides. PLoS One. 2012;7(9).
87. Joanne P, Galanth C, Goasdoué N, Nicolas P, Sagan S, Lavielle S, et al. Lipid reorganization induced by membrane-active peptides probed using differential scanning calorimetry. Biochim Biophys Acta - Biomembr. 2009;1788(9):1772–81.
88. Zhu WL, Shin SY. Antimicrobial and cytolytic activities and plausible mode of bactericidal action of the cell penetrating peptide penetratin and its Lys-linked two-stranded peptide. Chem Biol Drug Des. 2009;73(2):209–15.
89. Mouton JW, Meletiadis J, Voss A, Turnidge J. Variation of MIC measurements: The contribution of strain and laboratory variability to measurement precision. J Antimicrob Chemother. 2018;73(9):2374–9.
90. Rothbard JB, Jessop TC, Lewis RS, Murray BA, Wender PA. Role of membrane potential and hydrogen bonding in the mechanism of translocation of guanidinium-rich peptides into cells. J Am Chem Soc. 2004;126(31):9506–7.
91. Mitchell DJ, Steinman L, Kim DT, Fathman CG, Rothbard JB. Polyarginine enters cells more efficiently than other polycationic homopolymers. J Pept Res. 2000;56(5):318–25.
92. Fischer PM, Zhelev NZ, Wang S, Melville JE, Fåhraeus R, Lane DP. Structure-activity relationship of truncated and substituted analogues of the intracellular delivery vector Penetratin. J Pept Res. 2000;55(2):163–72.
93. Birch D, Christensen M V., Staerk D, Franzyk H, Nielsen HM. Stereochemistry as a determining factor for the effect of a cell-penetrating peptide on cellular viability and epithelial integrity. Biochem J. 2018;475(10):1773–88.
94. De La Fuente-Núñez C, Reffuveille F, Mansour SC, Reckseidler-Zenteno SL, Hernández D, Brackman G, et al. D-Enantiomeric Peptides that Eradicate Wild-Type and Multidrug-Resistant Biofilms and Protect against Lethal Pseudomonas aeruginosa Infections. Chem Biol. 2015 Feb 19;22(2):196–205.

95. Khafagy ES, Iwamae R, Kamei N, Takeda-Morishita M. Region-Dependent Role of Cell-Penetrating Peptides in Insulin Absorption Across the Rat Small Intestinal Membrane. AAPS J. 2015;17(6):1427–37.
96. Sousa F, Castro P, Fonte P, Sarmento B. How to overcome the limitations of current insulin administration with new non-invasive delivery systems. Ther Deliv. 2015;6(1):83–94.
97. Brown TD, Whitehead KA, Mitragotri S. Materials for oral delivery of proteins and peptides. Nat Rev Mater. 2020;5(2):127–48.
98. Kamei N, Shigei C, Hasegawa R, Takeda-Morishita M. Exploration of the Key Factors for Optimizing the in Vivo Oral Delivery of Insulin by Using a Noncovalent Strategy with Cell-Penetrating Peptides. Biol Pharm Bull. 2018;41(2):239–46.
99. Kamei N, Kikuchi S, Takeda-Morishita M, Terasawa Y, Yasuda A, Yamamoto S, et al. Determination of the optimal cell-penetrating peptide sequence for intestinal insulin delivery based on molecular orbital analysis with self-organizing maps. J Pharm Sci. 2013;102(2):469–79.
100. Iwase Y, Kamei N, Khafagy ES, Miyamoto M, Takeda-Morishita M. Use of a non-covalent cell-penetrating peptide strategy to enhance the nasal delivery of interferon beta and its PEGylated form. Int J Pharm. 2016;510(1):304–10.
101. Kristensen M, Nielsen HM. Cell-penetrating peptides as tools to enhance non-injectable delivery of biopharmaceuticals. Tissue Barriers. 2016;4(2):1–15.
102. Ward BP, Ottaway NL, Perez-Tilve D, Ma D, Gelfanov VM, Tschöp MH, et al. Peptide lipidation stabilizes structure to enhance biological function. Mol Metab. 2013;2(4):468–79.
103. Hedegaard SF, Bruhn DS, Khandelia H, Hedegaard SF, Bruhn DS, Khandelia H, et al. Shuffled lipidation pattern and degree of lipidation determines the membrane interaction behavior of a linear cationic membrane-active peptide. J Colloid Interface Sci. 2020;578.
104. Maher S, Mrsny RJ, Brayden DJ. Intestinal permeation enhancers for oral peptide delivery. Adv Drug Deliv Rev. 2016;106:277–319.
105. Lewis AL, Richard J. Challenges in the delivery of peptide drugs: An industry perspective. Ther Deliv. 2015;6(2):149–63.

106. Zhang J, Desale SS, Bronich TK. Polymer-based vehicles for therapeutic peptide delivery. Ther Deliv. 2015;6(11):1279–96.
107. Qi J, Gao R, Liu C, Shan B, Gao F, He J, et al. Potential role of the antimicrobial peptide tachyplesin III against multidrug-resistant P. aeruginosa and A. baumannii coinfection in an animal model. Infect Drug Resist. 2019;12:2865–74.
108. Niu C-H, Chiu Y-Y. FDA Perspective on Peptide Formulation and Stability Issues. J Pharm Sci. 1998;87(11):1331–4.
109. Nordström R, Malmsten M. Delivery systems for antimicrobial peptides. Adv Colloid Interface Sci. 2017;242:17–34.
110. de Alteriis E, Maselli V, Falanga A, Galdiero S, Di Lella FM, Gesuele R, et al. Efficiency of gold nanoparticles coated with the antimicrobial peptide indolicidin against biofilm formation and development of Candida spp. clinical isolates. Infect Drug Resist. 2018;11:915–25.
111. Pal I, Bhattacharyya D, Kar RK, Zarena D, Bhunia A, Atreya HS. A Peptide-Nanoparticle System with Improved Efficacy against Multidrug Resistant Bacteria. Sci Rep. 2019;9(1):1–11.
112. Sur A, Pradhan B, Banerjee A, Aich P. Immune activation efficacy of indolicidin is enhanced upon conjugation with carbon nanotubes and gold nanoparticles. PLoS One. 2015;10(4).
113. Braun K, Pochert A, Lindén M, Davoudi M, Schmidtchen A, Nordström R, et al. Membrane interactions of mesoporous silica nanoparticles as carriers of antimicrobial peptides. J Colloid Interface Sci. 2016;475:161–70.
114. Azharuddin M, Zhu GH, Das D, Ozgur E, Uzun L, Turner APF, et al. A repertoire of biomedical applications of noble metal nanoparticles. Chem Commun. 2019;55(49):6964–96.
115. Kaur J, Gill GS, Jeet K. Applications of carbon nanotubes in drug delivery: a comprehensive review. In: Characterization and biology of nanomaterials for drug delivery. Elsevier; 2018. p. 113–35.
116. Abed N, Couvreur P. Nanocarriers for antibiotics: A promising solution to treat intracellular bacterial infections. Int J Antimicrob Agents. 2014;43(6):485–96.
117. Ron-Doitch S, Sawodny B, Kühbacher A, David MMN, Samanta A, Phopase J, et al. Reduced cytotoxicity and enhanced bioactivity of cationic antimicrobial peptides liposomes in cell

cultures and 3D epidermis model against HSV. J Control Release. 2016;229:163–71.

118. Lopes NA, Pinilla CMB, Brandelli A. Pectin and polygalacturonic acid-coated liposomes as novel delivery system for nisin: Preparation, characterization and release behavior. Food Hydrocoll. 2017;70:1–7.

119. Da Silva IM, Boelter JF, Da Silveira NP, Brandelli A. Phosphatidylcholine nanovesicles coated with chitosan or chondroitin sulfate as novel devices for bacteriocin delivery. J Nanoparticle Res. 2014;16(7):2479.

120. Pu C, Tang W. A chitosan-coated liposome encapsulating antibacterial peptide, Apep10: Characterisation, triggered-release effects and antilisterial activity in thaw water of frozen chicken. Food Funct. 2016;7(10):4310–22.

121. Boge L, Bysell H, Ringstad L, Wennman D, Umerska A, Cassisa V, et al. Lipid-Based Liquid Crystals As Carriers for Antimicrobial Peptides: Phase Behavior and Antimicrobial Effect. Langmuir. 2016;32(17):4217–28.

122. Boge L, Browning KL, Nordström R, Campana M, Damgaard LSE, Seth Caous J, et al. Peptide-Loaded Cubosomes Functioning as an Antimicrobial Unit against Escherichia coli. ACS Appl Mater Interfaces. 2019;11(24):21314–22.

123. Gupta N, Rai DB, Jangid AK, Kulhari H. Use of nanotechnology in antimicrobial therapy. In: Ball A, Soni S, Gurtler V, editors. Methods in Microbiology: Nanotechnology. Academic Press; 2019. p. 143–72.

124. Du AW, Stenzel MH. Drug carriers for the delivery of therapeutic peptides. Biomacromolecules. 2014;15(4):1097–114.

125. Casciaro B, D'Angelo I, Zhang X, Loffredo MR, Conte G, Cappiello F, et al. Poly(lactide-co-glycolide) Nanoparticles for Prolonged Therapeutic Efficacy of Esculentin-1a-Derived Antimicrobial Peptides against Pseudomonas aeruginosa Lung Infection: In Vitro and in Vivo Studies. Biomacromolecules. 2019;20(5):1876–88.

126. Almaaytah A, Mohammed GK, Abualhaijaa A, Al-Balas Q. Development of novel ultrashort antimicrobial peptide nanoparticles with potent antimicrobial and antibiofilm activities against multidrug-resistant bacteria. Drug Des Devel Ther. 2017;11:3159–70.

127. Soto KM, Hernández-Iturriaga M, Loarca-Piña G, Luna-Bárcenas G, Mendoza S.

Antimicrobial effect of nisin electrospun amaranth: pullulan nanofibers in apple juice and fresh cheese. Int J Food Microbiol. 2019;295:25–32.

128. Kabanov A V, Vinogradov S V. Nanogels as Pharmaceutical Carriers: Finite Networks of Infinite Capabilities. Angew Chemie Int Ed. 2009;48(30):5418–29.
129. Cleophas RTC, Riool M, Quarles Van Ufford HC, Zaat SAJ, Kruijtzer JAW, Liskamp RMJ. Convenient preparation of bactericidal hydrogels by covalent attachment of stabilized antimicrobial peptides using thiol-ene click chemistry. ACS Macro Lett. 2014;3(5):477–80.
130. Water JJ, Kim Y, Maltesen MJ, Franzyk H, Foged C, Nielsen HM. Hyaluronic acid-based nanoge ls produced by microfluidics-facilitated self-assembly improves the safety profile of the cationic host defense peptide novicidin. Pharm Res. 2015;32(8):2727–35.
131. Salimi A, Makhmalzadeh BS, Esfahani G. Polymeric Micelle as a New Carrier in Oral Drug Delivery Systems. Asian J Pharm. 2017;11(4):S704–11.
132. Weissmann B, Meyer K. The Structure of Hyalobiuronic Acid and of Hyaluronic Acid from Umbilical Cord. J Am Chem Soc. 1954;76(7):1753–7.
133. Šmejkalová D, Muthný T, Nešporová K, Hermannová M, Achbergerová E, Huerta-Angeles G, et al. Hyaluronan polymeric micelles for topical drug delivery. Carbohydr Polym. 2017 Jan 20;156:86–96.
134. Nešporová K, Šógorková J, Šmejkalová D, Kulhánek J, Huerta-Angeles G, Kubala L, et al. Influence of serum albumin on intracellular delivery of drug-loaded hyaluronan polymeric micelles. Int J Pharm. 2016 Sep 10;511(1):638–47.
135. Lequeux I, Ducasse E, Jouenne T, Thebault P. Addition of antimicrobial properties to hyaluronic acid by grafting of antimicrobial peptide. Eur Polym J. 2014;51(1):182–90.
136. Ardizzoni A, Neglia RG, Baschieri MC, Cermelli C, Caratozzolo M, Righi E, et al. Influence of hyaluronic acid on bacterial and fungal species, including clinically relevant opportunistic pathogens. J Mater Sci Mater Med. 2011;22(10):2329–38.
137. Šmejkalová D, Nešporová K, Hermannová M, Huerta-Angeles G, Čožíková D, Vištejnová L, et al. Paclitaxel isomerisation in polymeric micelles based on hydrophobized hyaluronic acid. Int J Pharm. 2014;466(1–2):147–55.
138. Khunmanee S, Jeong Y, Park H. Crosslinking method of hyaluronic-based hydrogel for

biomedical applications. J Tissue Eng. 2017;8:2041731417726464.

139. Silva JP, Gonçalves C, Costa C, Sousa J, Silva-Gomes R, Castro AG, et al. Delivery of LLKKK18 loaded into self-assembling hyaluronic acid nanogel for tuberculosis treatment. J Control Release. 2016 Aug 10;235:112–24.

140. Kłodzińska SN, Molchanova N, Franzyk H, Hansen PR, Damborg P, Nielsen HM. Biopolymer nanogels improve antibacterial activity and safety profile of a novel lysine-based α-peptide/β-peptoid peptidomimetic. Eur J Pharm Biopharm. 2018 Jul 1;128:1–9.

141. Kłodzińska SN, Pletzer D, Rahanjam N, Rades T, Hancock REW, Nielsen HM. Hyaluronic acid-based nanogels improve in vivo compatibility of the anti-biofilm peptide DJK-5. Nanomedicine Nanotechnology, Biol Med. 2019;20(06).

142. Wei X, Senanayake TH, Warren G, Vinogradov S V. Hyaluronic acid-based nanogel-drug conjugates with enhanced anticancer activity designed for the targeting of cd44-positive and drug-resistant tumors. Bioconjug Chem. 2013;24(4):658–68.

143. Choi K mi, Jang M, Kim JH, Ahn HJ. Tumor-specific delivery of siRNA using supramolecular assembly of hyaluronic acid nanoparticles and 2b RNA-binding protein/siRNA complexes. Biomaterials. 2014 Aug 1;35(25):7121–32.

144. Huerta-Angeles G, Bobek M, Příkopová E, Šmejkalová D, Velebný V. Novel synthetic method for the preparation of amphiphilic hyaluronan by means of aliphatic aromatic anhydrides. Carbohydr Polym. 2014;111:883–91.

145. Clawson C, Ton L, Aryal S, Fu V, Esener S, Zhang L. Synthesis and characterization of lipid-polymer hybrid nanoparticles with pH-triggered PEG shedding. Langmuir. 2008;27(17):10556–61.

146. Abdelaziz AA, Elbanna TE, Sonbol FI, Gamaleldin NM, El Maghraby GM. Optimization of niosomes for enhanced antibacterial activity and reduced bacterial resistance: in vitro and in vivo evaluation. Expert Opin Drug Deliv. 2015;12(2):163–80.

147. Jackman JA, Yoon BK, Li D, Cho NJ. Nanotechnology formulations for antibacterial free fatty acids and monoglycerides. Molecules. 2016;21(3):1–19.

148. Speert DP, Wannamaker LW, Gray ED, Clawson CC. Bactericidal effect of oleic acid on group A streptococci: Mechanism of action. Infect Immun. 1979;26(3):1202–10.

149. Taylor SL, Wahl-Jensen V, Copeland AM, Jahrling PB, Schmaljohn CS. Endothelial cell permeability during hantavirus infection involves factor XII-dependent increased activation of the kallikrein-kinin system. PLoS Pathog. 2013;9(7):e1003470.
150. Lee WL, Liles WC. Endothelial activation, dysfunction and permeability during severe infections. Curr Opin Hematol. 2011;18(3):191–6.
151. Azzopardi EA, Ferguson EL, Thomas DW. The enhanced permeability retention effect: a new paradigm for drug targeting in infection. J Antimicrob Chemother. 2013;68(2):257–74.
152. Gao W, Thamphiwatana S, Angsantikul P, Zhang L. Nanoparticle approaches against bacterial infections. Wiley Interdiscip Rev Nanomed Nanobiotechnol. 2014;6(6):532–47.
153. Tee JK, Li A, Yip X, Tan ES, Santitewagun S, Prasath A, et al. Nanoparticles' interactions with vasculature in diseases Chem Soc Rev. Chem Soc Rev. 2019;48:5381–407.
154. Wei Y, Quan L, Zhou C, Zhan Q. Factors relating to the biodistribution & clearance of nanoparticles & their effects on in vivo application. Vol. 13, Nanomedicine. Future Medicine Ltd.; 2018. p. 1495–512.
155. Hoshyar N, Gray S, Han H, Bao G. The effect of nanoparticle size on in vivo pharmacokinetics and cellular interaction. Nanomedicine (Lond). 2016 Mar;11(6):673–92.
156. Kulkarni SA, Feng S-S. Effects of Particle Size and Surface Modification on Cellular Uptake and Biodistribution of Polymeric Nanoparticles for Drug Delivery.
157. Cuggino JC, Blanco ERO, Gugliotta LM, Igarzabal CIA, Calderón M. Crossing biological barriers with nanogels to improve drug delivery performance. J Control Release. 2019;307:221–46.
158. Harush-Frenkel O, Bivas-Benita M, Nassar T, Springer C, Sherman Y, Avital A, et al. A safety and tolerability study of differently-charged nanoparticles for local pulmonary drug delivery. Toxicol Appl Pharmacol. 2010 Jul 1;246(1–2):83–90.
159. Le MQ, Carpentier R, Lantier I, Ducournau C, Dimier-Poisson I, Betbeder D. Residence time and uptake of porous and cationic maltodextrin-based nanoparticles in the nasal mucosa: comparison with anionic and cationic nanoparticles. Int J Pharm. 2018;550(1–2):316–24.
160. Kim Y, Lee Chung B, Ma M, Mulder WJM, Fayad ZA, Farokhzad OC, et al. Mass Production and Size Control of Lipid–Polymer Hybrid Nanoparticles through Controlled Microvortices.

Nano Lett. 2012;12(7):3587–91.

161. Schneider CA, Rasband WS, Eliceiri KW. NIH Image to ImageJ: 25 years of image analysis. Nat Methods. 2012;9(7):671–5.

162. Institute C and LS. Methods for dilution antimicrobial susceptibility tests for bacteria that grow aerobically; approved standard. Vol. 32, CLSI document M07-A9. Clinical and Laboratory Standards Institute Wayne, PA; 2012.

163. Chen H, Wubbolts RW, Haagsman HP, Veldhuizen EJA. Inhibition and Eradication of Pseudomonas aeruginosa Biofilms by Host Defence Peptides. Sci Rep. 2018 Jul;8(1):10446.

164. Joshi DR, Adhikari N. An overview on common organic solvents and their toxicity. J Pharm Res Int. 2019;1–18.

165. Průšová A, Vergeldt FJ, Kučerík J. Influence of water content and drying on the physical structure of native hyaluronan. Carbohydr Polym. 2013 Jun;95(1):515–21.

166. Chiesa E, Dorati R, Conti B, Modena T, Cova E, Meloni F, et al. Molecular Sciences Hyaluronic Acid-Decorated Chitosan Nanoparticles for CD44-Targeted Delivery of Everolimus. 2018.

167. Hussain Z, Pandey M, Choudhury H, Ying PC, Xian TM, Kaur T, et al. Hyaluronic acid functionalized nanoparticles for simultaneous delivery of curcumin and resveratrol for management of chronic diabetic wounds: Fabrication, characterization, stability and in vitro release kinetics. J Drug Deliv Sci Technol. 2020 Jun 1;57:101747.

168. Thomas D, Latha MS, Thomas KK. Synthesis and in vitro evaluation of alginate-cellulose nanocrystal hybrid nanoparticles for the controlled oral delivery of rifampicin. J Drug Deliv Sci Technol. 2018 Aug 1;46:392–9.

169. Ghomrasni NB, Chivas-Joly C, Devoille L, Hochepied J-F, Feltin N. Challenges in sample preparation for measuring nanoparticles size by scanning electron microscopy from suspensions, powder form and complex media. Powder Technol. 2020;359:226–37.

170. Ghaderi S, Ghanbarzadeh S, Hamishehkar H. Evaluation of different methods to produce nanoparticle containing gammaoryzanol for potential use in food fortification. Pharm Sci. 2014;20(4):130–4.

171. Zhang H. Thin-film hydration followed by extrusion method for liposome preparation. In:

Methods in Molecular Biology. Humana Press Inc.; 2017. p. 17–22.

172. Jahn A, Vreeland WN, Devoe DL, Locascio LE, Gaitan M. Microfluidic directed formation of liposomes of controlled size. Langmuir. 2007 May 22;23(11):6289–93.

173. Jahn A, Vreeland WN, Gaitan M, Locascio LE. Controlled Vesicle Self-Assembly in Microfluidic Channels with Hydrodynamic Focusing. J Am Chem Soc. 2004;126(9):2674–5.

174. Zhao CX, Middelberg APJ. Two-phase microfluidic flows. Chem Eng Sci. 2011 Apr 1;66(7):1394–411.

175. Bicudo RCS, Santana MHA. Production of hyaluronic acid (HA) nanoparticles by a continuous process inside microchannels: Effects of non-solvents, organic phase flow rate, and HA concentration. Chem Eng Sci. 2012 Dec 24;84:134–41.

176. Kłodzińska SN, Wan F, Jumaa H, Sternberg C, Rades T, Nielsen HM. Utilizing nanoparticles for improving anti-biofilm effects of azithromycin: A head-to-head comparison of modified hyaluronic acid nanogels and coated poly (lactic-co-glycolic acid) nanoparticles. J Colloid Interface Sci. 2019 Nov 1;555:595–606.

177. Yoon J-Y, Garrell RL. Biomolecular Adsorption in Microfluidics. In: Encyclopedia of Microfluidics and Nanofluidics. Springer US; 2008. p. 68–76.

178. Tomaszewska E, Soliwoda K, Kadziola K, Tkacz-Szczesna B, Celichowski G, Cichomski M, et al. Detection limits of DLS and UV-Vis spectroscopy in characterization of polydisperse nanoparticles colloids. J Nanomater. 2013;2013.

179. Stetefeld J, McKenna SA, Patel TR. Dynamic light scattering: a practical guide and applications in biomedical sciences. Biophys Rev. 2016;8(4):409–27.

180. Kumar G, Shafiq N, Malhotra S. Drug-loaded PLGA nanoparticles for oral administration: fundamental issues and challenges ahead. Crit Rev Ther Drug Carr Syst. 2012;29(2).

181. Walkey CD, Olsen JB, Guo H, Emili A, Chan WCW. Nanoparticle size and surface chemistry determine serum protein adsorption and macrophage uptake. J Am Chem Soc. 2012;134(4):2139–47.

182. Instruments M. Zetasizer Nano User Manual MAN0317. Malvern Instruments Ltd Malvern, United Kingdom. 2009;5:1–12.

183. Trevisan JE, Cavalcanti LP, Oliveira CLP, De La Torre LG, Santana MHA. Technological

aspects of scalable processes for the production of functional liposomes for gene therapy. Non-viral gene Ther Intech. 2011;267–92.

184. Mohanraj VJ, Chen Y. Nanoparticles: a review. Trop J Pharm Res. 2006;5(1):561–73.

185. Almalik A, Alradwan I, Kalam MA, Alshamsan A. Effect of cryoprotection on particle size stability and preservation of chitosan nanoparticles with and without hyaluronate or alginate coating. Saudi Pharm J. 2017 Sep 1;25(6):861–7.

186. Beirowski J, Inghelbrecht S, Arien A, Gieseler H. Freeze-drying of nanosuspensions, 1: Freezing rate versus formulation design as critical factors to preserve the original particle size distribution. J Pharm Sci. 2011 May 1;100(5):1958–68.

187. Chen Y, Guarnieri MT, Vasil AI, Vasil ML, Mant CT, Hodges RS. Role of peptide hydrophobicity in the mechanism of action of α-helical antimicrobial peptides. Antimicrob Agents Chemother. 2007 Apr;51(4):1398–406.

188. Balows A. Current techniques for antibiotic susceptibility testing. Charles C. Thomas Publisher; 1974.

189. Malanovic N, Lohner K. Gram-positive bacterial cell envelopes: The impact on the activity of antimicrobial peptides. Biochim Biophys Acta - Biomembr. 2016;1858(5):936–46.

190. Manabe T, Kawasaki K. D-form KLKLLLLLKLK-NH 2 peptide exerts higher antimicrobial properties than its L-form counterpart via an association with bacterial cell wall components. Sci Rep. 2017;7(1):1–10.

191. Cieplik F, García-Contreras R, Van Hoek ML, Olivares E, Badel-Berchoux S, Provot C, et al. Clinical Impact of Antibiotics for the Treatment of Pseudomonas aeruginosa Biofilm Infections. 2020.

192. Mirani ZA, Fatima A, Urooj S, Aziz M, Khan MN, Abbas T. Relationshipof cell surfacehydrophobicitywithbiofilmformationand growth rate: A study on Pseudomonas aeruginosa, Staphylococcus aureus, and Escherichia coli. Iran J Basic Med Sci. 2018 Jul;21(7):760–9.

193. Flemming H-C, Wingender J, Szewzyk U, Steinberg P, Rice SA, Kjelleberg S. Biofilms: an emergent form of bacterial life. Nat Rev Microbiol. 2016;14(9):563–75.

194. Eleraky NE, Allam A, Hassan SB, Omar MM. Nanomedicine Fight against Antibacterial

Resistance: An Overview of the Recent Pharmaceutical Innovations. Pharmaceutics. 2020 Feb 8;12(2):142.

195. Ilomuanya MO, Elesho RF, Amenaghawon AN, Adetuyi AO, Velusamy V, Akanmu AS. Development of trigger sensitive hyaluronic acid/palm oil-based organogel for in vitro release of HIV/AIDS microbicides using artificial neural networks. Futur J Pharm Sci. 2020 Dec;6(1):1.

196. Bayer IS. Hyaluronic Acid and Controlled Release: A Review. Molecules. 2020 Jun;25(11):2649.

8. Appendix

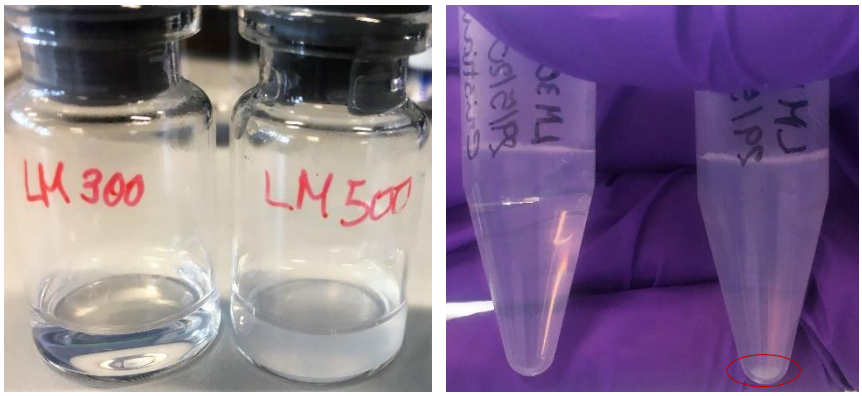

Figure 18 – Comparison between the L-Pmax to OL-HA ratio, evidencing the aggregation and sedimentation of the nanoparticles of the highest ratio (red circle). In each image, in the left is 0.3 ratio and in the 0.5 ratio.

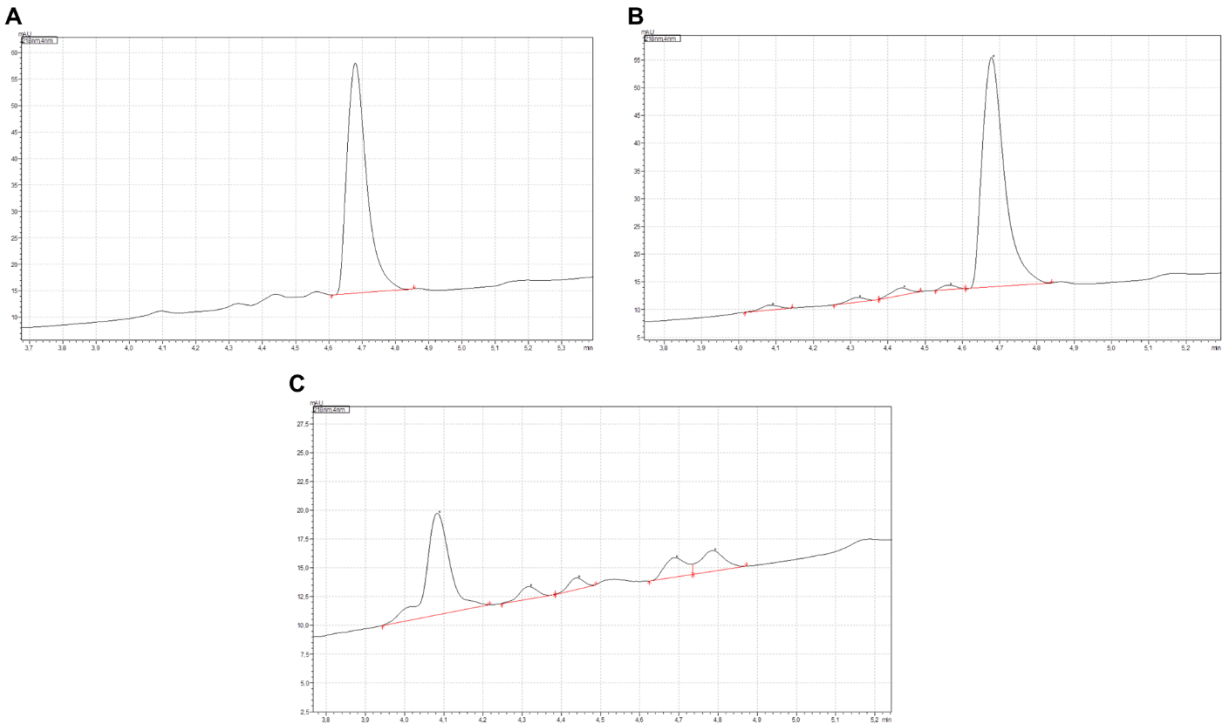

Figure 19 - HPLC chromatograms of the release study: (**A**) concentration of 20 µg/mL L-Pmax in HEPES pH 7.4, normal retention peak at 4.7 min (**B**) L-Pmax control after 8 h of release and (**C**) 48 h after. Xx axis is the retention time and yy axis is the absorption intensity.

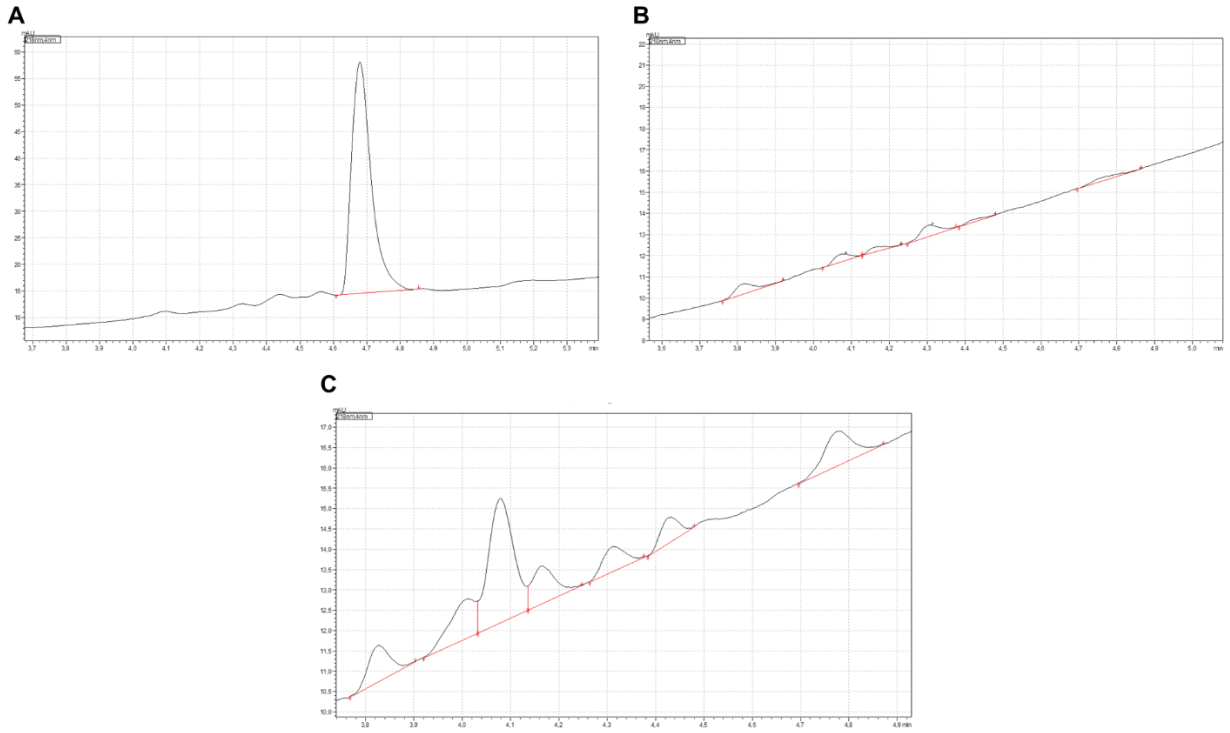

Figure 20 - HPLC chromatograms of the release study: (**A**) concentration of 20 µg/mL L-Pmax in HEPES pH 7.4, normal retention peak at 4.7 min (**B**) Release of L-Pmax from the OL-HA(L-Pmax) micelles after 8 h of release and (**C**) 24 h after. Xx axis is the retention time and yy axis is the absorption intensity.

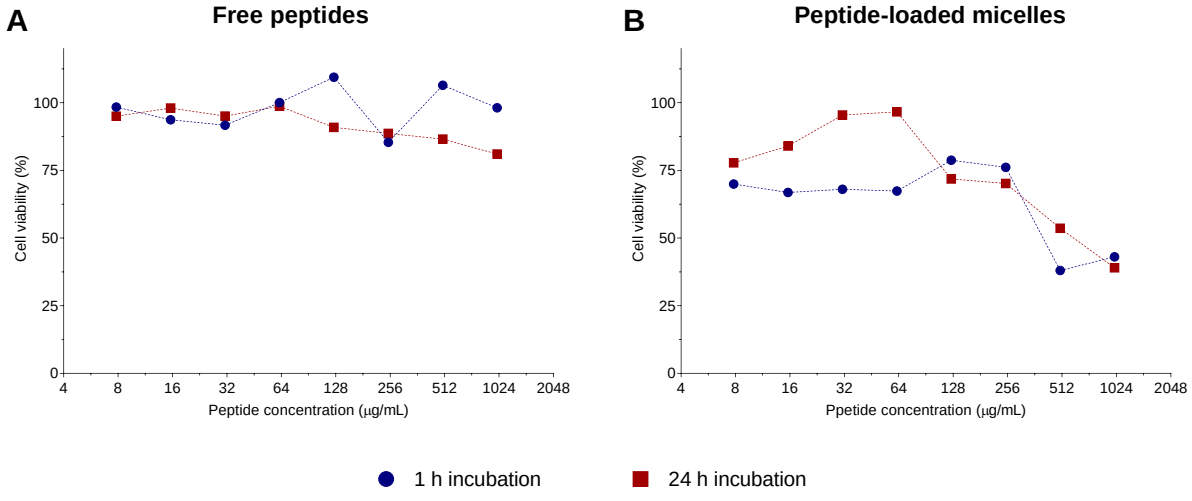

Figure 21 – Cytotoxicity towards (**A**) HepG2 and (**B**) HUVEC cells of empty OL-HA micelles, after 1h and 24 h incubation; using MTS assay and represented as % cell viability related to the untreated control. N=1